

Trinity University

Digital Commons @ Trinity

Geosciences Faculty Research

Geosciences Department

6-2020

Controls on Microbial and Oolitic Carbonate Sedimentation and Stratigraphic Cyclicity Within a Mixed Carbonate-Siliciclastic System: Upper Cambrian Wilberns Formation, Llano Uplift, Mason County, Texas, USA

Daniel J. Lehrmann

Trinity University, dlehrman@trinity.edu

A. W. Droxler

P. Harris

M. Minzoni

Dylan A. Droxler

Trinity University, ddroxler@trinity.edu

See next page for additional authors

Follow this and additional works at: https://digitalcommons.trinity.edu/geo_faculty



Part of the [Earth Sciences Commons](#)

Repository Citation




Lehrmann, D. J., Droxler, A. W., Harris, P., Minzoni, M., Droxler, D. A., Hopson, H. H., Kelleher, C., ... & Yazbek, L. (2020). Controls on microbial and oolitic carbonate sedimentation and stratigraphic cyclicity within a mixed carbonate-siliciclastic system: Upper Cambrian Wilberns Formation, Llano Uplift, Mason County, Texas, USA. *Depositional Record*, 6(2), 276-308. <http://doi.org/10.1002/dep2.108>

This Article is brought to you for free and open access by the Geosciences Department at Digital Commons @ Trinity. It has been accepted for inclusion in Geosciences Faculty Research by an authorized administrator of Digital Commons @ Trinity. For more information, please contact jcostanz@trinity.edu.

Authors

Daniel J. Lehrmann, A. W. Droxler, P. Harris, M. Minzoni, Dylan A. Droxler, H. H. Hopson, Caroline Kelleher, P. Khanna, Asmara A. Lehrmann, Adrien Lhemann, Grace Mabry, Lauren Mercado, J. M. Proctor, Pulkit Singh, and Lindsey D. Yazbek

Controls on microbial and oolitic carbonate sedimentation and stratigraphic cyclicity within a mixed carbonate-siliciclastic system: Upper Cambrian Wilberns Formation, Llano Uplift, Mason County, Texas, USA

Daniel J. Lehrmann¹  | André W. Droxler² | Paul (Mitch) Harris³  |
 Marcello Minzoni⁴ | Dylan A. Droxler¹ | Heath H. Hopson² | Caroline Kelleher¹ |
 Pankaj Khanna²  | Asmara A. Lehrmann¹ | Adrien Lhemann¹ | Grace Mabry¹ |
 Lauren Mercado¹ | Jacob M. Proctor² | Pulkit Singh² | Lindsey Yazbek¹

¹Geosciences Department, Trinity University, San Antonio, TX, USA

²Department of Earth Science, Rice University, Houston, TX, USA

³CSL – Center for Carbonate Research, University of Miami RSMAS, Miami, FL, USA

⁴Department of Geological Sciences, The University of Alabama, Tuscaloosa, AL, USA

Correspondence

Daniel J. Lehrmann, Geosciences Department, Trinity University, One Trinity Place, San Antonio, TX 78212, USA.
 Email: dlehrmann@trinity.edu

Funding information

Chevron; Conoco-Phillips; Shell; Statoil; Rice University Subcontract, Grant/Award Number: OTT-SRA-13-0182_Sub

Abstract

The upper Cambrian Wilberns Formation in central Texas records deposition on a low-gradient shelf within a mixed carbonate–siliciclastic tidal-flat system that changes offshore to subtidal shelf and open-marine oolitic skeletal shoals with large microbial mounds. Siliciclastic sediment is interpreted to have been delivered to the tidal flat by aeolian processes because of the narrow range in grain size and paucity of clay. Tidal influence is dominant as evidenced by reversing currents and desiccation on the tidal flat, and megaripples with reversing current indicators in offshore shoals. Intraclastic conglomerates were deposited in broad channels on the tidal flats during storm surges. Microbialite deposition is interpreted to be controlled by accommodation favouring amalgamated thin biostromes developed in the tidal flat vs. larger mounds with greater synoptic relief in the offshore, and current energy resulting in preferential elongation of offshore mounds in a NE–SW orientation. Intertidal mounds and biostromes grew in the presence of significant siliciclastic flux and trapped it within their structure, whereas offshore large buildups incorporated little siliciclastic component. Oolite and skeletal grainstone formed in tide agitated shoals associated with large subtidal microbial mounds. Storms extensively recycled and redistributed skeletal and oolitic sands from the offshore shoals across the shelf as thin sand sheets. Spatial mixing of siliciclastic and carbonate sediment occurred across the tidal flat and shelf. Low-frequency and intermediate-frequency stratigraphic cycles were driven by shifts in the shoreline and changes in rate of siliciclastic flux in response to relative sea-level fluctuation. Random facies stacking and the lack of metre-scale cyclicity are interpreted to reflect stratigraphic incompleteness and an episodic signal introduced by storms.

This is an open access article under the terms of the Creative Commons Attribution License, which permits use, distribution and reproduction in any medium, provided the original work is properly cited.

© 2020 The Authors. *The Depositional Record* published by John Wiley & Sons Ltd on behalf of International Association of Sedimentologists.

KEYWORDSCambrian, carbonate, *Laurentia*, microbialite, oolite, siliciclastic**1 | INTRODUCTION**

Marine microbialite and oolitic carbonate sediments are important proxies for physical, chemical and biological environmental conditions in the rock record. Microbial and oolitic carbonates are also fundamental components of two distinct benthic carbonate factory types, or modes of carbonate sediment production, that reflect environmental parameters, water depth and production potential (Schlager, 2000, 2003; Reijmer, 2014). Furthermore, microbial and oolitic facies have received intensive sedimentological study as they are common hydrocarbon reservoirs across the geologic column (e.g. Cambro-Ordovician, Permian, Triassic, Jurassic) hosting some of the world's most prolific hydrocarbon fields (Mancini *et al.*, 2013 and references therein).

The widespread interest in microbial and oolitic carbonates has resulted in improved understanding of the environmental factors controlling their genesis. Studies of modern marine microbial carbonate mounds have constrained their morphologies and microscopic structures and elucidated the physical and chemical factors affecting their morphology, growth substrates, microbial communities and their role in sediment trapping/binding and precipitation, together with the taphonomic processes affecting preservation (Dill *et al.*, 1986; Reid *et al.*, 1995, 2003; Ginsburg and Planavsky, 2008; Planavsky and Ginsburg, 2009; Dupraz *et al.*, 2011; Suosaari *et al.*, 2016). Studies of ancient microbial carbonates have identified microscopic, mesoscopic and macroscopic internal structures, secular trends in microbial forms and abundance across geologic history vs. change in environmental factors such as climate, seawater chemistry and biotic evolution, and environmental factors effecting growth forms (Rowland and Shapiro, 2002; Riding and Liang, 2005; Riding, 2006, 2011; Kiessling, 2009; Bosak *et al.*, 2013). Similarly, studies of modern and ancient oolitic carbonates have advanced understanding of the microstructure of ooids, physical and biochemical controls on precipitation and sedimentary structures, and secular trends in morphology and mineralogy across Earth history vs. chemical and environmental factors (Wilkinson *et al.*, 1985; Sumner and Grotzinger, 1993; Trower *et al.*, 2017; Harris *et al.*, 2019). Despite these advances, it is still uncertain what environmental factors (such as seawater carbonate saturation, biological factors, siliciclastic input, accommodation space or current energy) played dominant roles on precipitation, deposition and heterogeneity of microbialite and oolite deposits. Analysis of microbialite and oolite in the context of environmental indicators of associated facies in ancient depositional systems promises to help identify the constraints on genesis.

The occurrence of extensive flat-pebble conglomerates in carbonates preceding the Middle Ordovician has been interpreted as promotion by the high seawater carbonate saturation state and reduced depth of bioturbation prior to the great Ordovician biodiversification event (Wright and Cherns, 2016). However, a variety of mechanisms have been proposed for the formation of flat-pebble conglomerates and there is no consensus on their primary mode of genesis (Demicco and Hardie, 1995; Myrow *et al.*, 2004; Alvaro and Clausen, 2007; Pratt and Bordonaro, 2007). Further detailed analysis of Cambrian examples promises to better constrain their origins.

Cambrian–Ordovician strata of the Great American Carbonate Bank (GACB) are important for evaluating the controls on mixed carbonate–siliciclastic depositional systems in epicratonic seas (Cowan and James, 1993; Spencer and Demicco, 2002; Morgan, 2012; Runkel *et al.*, 2012; Labaj and Pratt, 2016), the role of tides, storms and other hydrodynamic currents such as gravity flows and tsunamis on shelf sedimentation (Pratt, 2002; Tape *et al.*, 2003; Myrow *et al.*, 2004; Eoff, 2014; MacNaughton *et al.*, 2019), and mechanisms impacting the record of high-frequency stratigraphic cyclicity (Demicco, 1985; Koerschner and Read, 1989; Goldhammer *et al.*, 1993; Cowan and James, 1996; Lehrmann and Goldhammer, 1999; Runkel *et al.*, 2007, 2008). However, previous studies have focussed on geographic areas other than central Texas, and there is a need for quantitative analysis of sediment composition and spatial mixing of carbonate and siliciclastics during deposition and the levels of order vs. randomness in cyclicity. Moreover, there is a need for analysis of the roles of sea-level fluctuation, siliciclastic flux and sediment reworking by currents in such depositional systems.

Previous studies of the upper Cambrian carbonates in the Llano area (central Texas) have mainly focussed on regional facies, stratigraphic mapping and biostratigraphy (Bridge *et al.*, 1947; Sliger, 1955; Barnes and Bell, 1977; Miller *et al.*, 2012), with only a few studies on the microbial reef structures and palaeoecology (Ahr, 1967, 1971; Ruppel and Kerans, 1987; Spincer, 1997). The authors recent research efforts have included detailed characterization of the smaller microbial mounds and biostromes of the lower Point Peak Member, the larger microbial buildups and associated sediments in the upper Point Peak Member, and detailed characterization of the facies succession of the upper Morgan Creek Member and Point Peak Member of the Wilberns Formation in the area along the Llano and James rivers, and Mill Creek south-west of Mason, Texas (Kelleher *et al.*, 2017; Khanna *et al.*, 2019; Proctor *et al.*, 2019).

The purpose of this paper is to provide an analysis of the environmental mechanisms controlling the genesis of

microbialites, oolites and other deposits such as flat-pebble conglomerates, and the controls on cyclicity, in the Wilberns Formation through evaluation of the environmental constraints provided by sedimentary structures and sediment composition in detailed stratigraphic sections of a mixed carbonate–siliciclastic system.

2 | GEOLOGIC SETTING

The upper Morgan Creek and Point Peak members of the Wilberns Formation of the upper Cambrian Moore Hollow Group crop out along the Llano and James rivers, and Mill Creek in the south-west portion of the Llano Uplift in Mason County central Texas (Figure 1). Biostratigraphy based on trilobites and conodonts at a continuous section exposed at Threadgill Creek, developed south-east of the subject field area, places the Wilberns Formation in the Sunwaptan Stage of the Furongian (Millardian) Series (Figure 1; Miller *et al.*,

2012). Cambrian carbonate, sandstone and siltstone strata are widely exposed around the periphery of the Llano Uplift where they unconformably overlie the Mesoproterozoic igneous and metamorphic basement (Figure 1A,B). The overall Cambrian–Early Ordovician facies succession is transgressive and contains a progressively greater carbonate content upward as epicontinental seas flooded Laurentia during the Sauk megasequence (Morgan, 2012; Figure 1B). The Sauk megasequence can be subdivided into three supersequences (Palmer, 1981; Morgan, 2012). In the Llano area, the Sauk II supersequence is recorded within the Riley Formation, whereas the Sauk III supersequence is recorded in the Wilberns Formation (Miller *et al.*, 2012; Morgan, 2012).

The Hickory Sandstone Member of the Riley Formation is terrestrial to marine and represents the initial transgression of the Sauk II sequence followed by the Cap Mountain Limestone Member, consisting of a regressive succession of limestone, sandstone and siltstone, and, finally, the Lion Mountain Member (Barnes and Bell, 1977; McBride *et al.*,

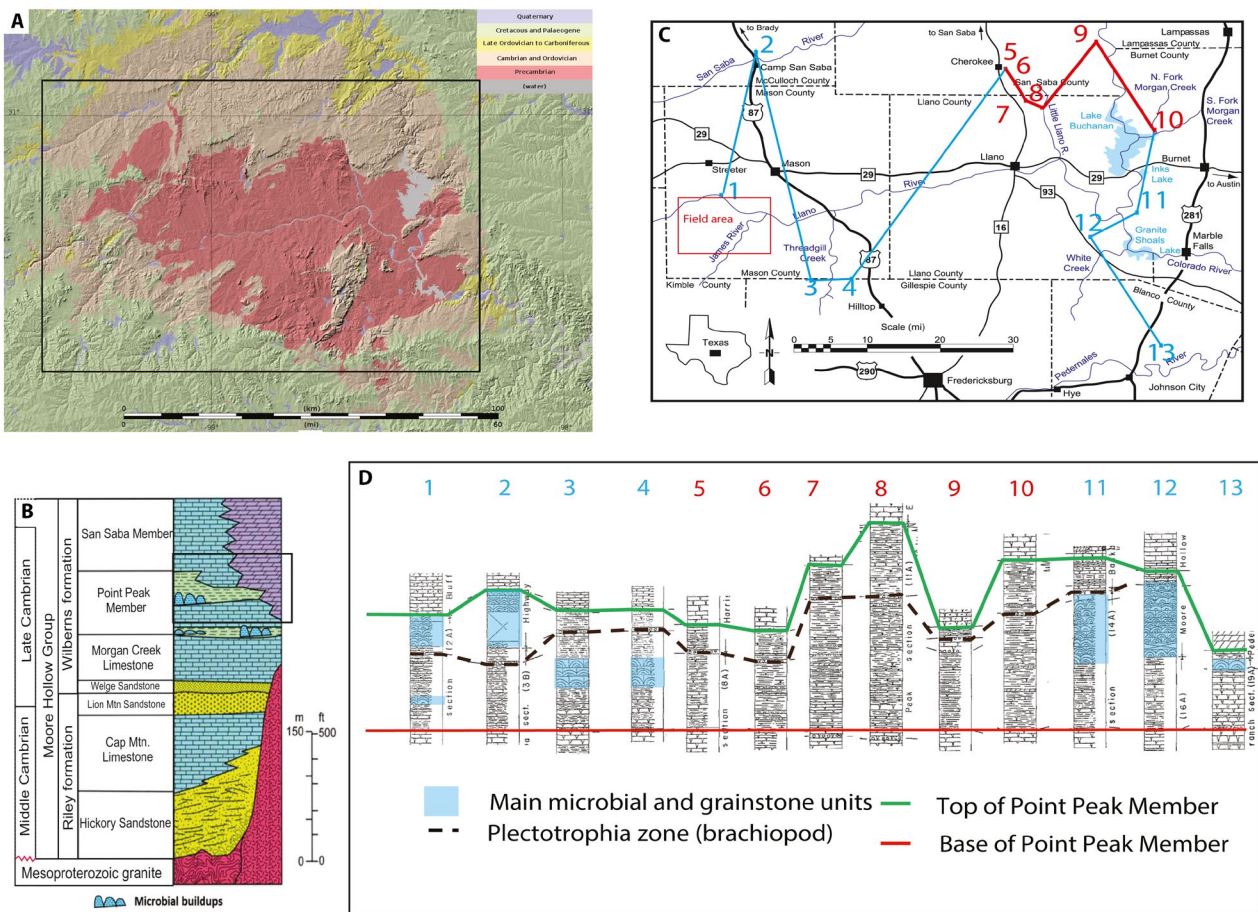


FIGURE 1 (A) Simplified geologic map of the Llano Area (compiled from USGS national geologic map database). Rectangle shows area of location map in (C). (B) Stratigraphic column for Cambrian strata of the Llano Uplift (modified from Barnes and Bell, 1977; Kyle and McBride, 2012). (C) Location map of stratigraphic cross section (modified from Miller *et al.*, 2012). Numbers indicating sections containing microbial carbonate are coloured in blue, whereas those composed of siliciclastic facies are red. (D) Stratigraphic cross section of the Point Peak Member of the Wilberns Formation (modified from Bridge *et al.*, 1947; Ahr, 1967). Location of sections is shown in (C). Microbial carbonates highlighted in blue on sections. Sections containing microbial carbonate are numbered in blue, whereas sections composed of siliciclastic facies are numbered in red

2002; Kyle and McBride, 2012). The Hickory Sandstone is composed of arkose, subarkose and diagenetic quartz arenite with variable rounding and grains with crescentic shapes indicative of aeolian transport (McBride *et al.*, 2002; Kyle and McBride, 2012). The sand is interpreted to have been sourced from the weathered basement of the Llano Uplift. Detrital zircon geochronology of the Hickory Sandstone provides ages consistent with sediment derivation from the Llano basement (Jones and Surpless, 2018).

The contact between the Riley and Wilberns formations, at the base of the Welge Sandstone Member, is a disconformity throughout the Llano area and is interpreted to be a supersequence boundary defining the base of the Sauk III sequence (Krause, 1996; Morgan, 2012). The Welge Sandstone Member records the initial transgressive deposit above the supersequence boundary. The Morgan Creek, Point Peak and San Saba members also reflect an overall transgression with thick microbial mounds developed in the Point Peak Member and a progressive reduction in siliciclastic content and eventual shift to dominant carbonate content during deposition of the San Saba Member and Ellenberger Group (Figure 1B; Kyle and McBride, 2012). Presumably, siliciclastic sand of the Lion Mountain and Wedge Sandstone members may have been sourced by the local Llano Precambrian igneous and metamorphic basement, although by the time of deposition of the Morgan Creek Member, much of the Llano basement may have been buried by marine deposits (Figure 1B).

During the Cambrian, the North American craton straddled the equator and was flanked on all sides by passive continental margins developed as a result of the Neoproterozoic breakup of Rodinia. During the Late Cambrian and Early Ordovician, under greenhouse climate conditions, rising sea level had flooded large parts of the continent forming widespread epeiric seas (Lochman-Balk, 1970). Siliciclastic sediments were shed from low-relief uplands such as the transcontinental arch forming an inner detrital belt, and tropical climate conditions stimulated widespread carbonate deposition of a vast, shallow-marine carbonate platform of the GACB (Ginsburg, 1982; Wilson, 1994; Bohacs *et al.*, 2012; Runkel *et al.*, 2012).

Previous studies have interpreted the palaeogeography of the Llano area during Wilberns deposition to either include a shoreline to the west with offshore deposition towards the east (Ahr, 1967), a shoreline to the north, with a E–W trending microbial reef barrier and offshore sedimentation to the south (Spincer, 1997) or a trend from nearshore to the north-east to offshore to the south-west (Ruppel and Kerans, 1987). Sections within Lampasas and San Saba counties in the north-east part of the Llano area are composed of siliciclastic sand and siltstone and lack carbonate strata (Figure 1C,D). Furthermore, this area has been interpreted as the largest upland bedrock area of the Llano Uplift and the source of siliciclastic flux to earlier Hickory Sandstone deposition (McBride *et al.*, 2002, p. 3). A

local uplift in this area likely persisted as islands contributing siliciclastic sediment and affecting the shoreline configuration during Morgan Creek and Point Peak deposition. Isopach maps of the Wilberns Formation indicate that the Point Peak Member thickens into depocentres to the south-east and south-west of the subject field area (Barnes and Bell, 1977). The Point Peak Member thins and is truncated 160 km to the west on the Texas Arch, an upland extension of the Transcontinental Arch in west Texas (Barnes and Bell, 1977). The Wilberns Formation was thus deposited in a vast, low-gradient epicratonic carbonate ramp with a distant shoreline to the west and a local shoreline and siliciclastic source area in the north-east of the subject field area in the Llano Uplift (Figure 1C).

3 | METHODS

Detailed overlapping stratigraphic sections were described bed-by-bed at the centimetre-scale from the Shepard Pavement (Llano River), Lower Mill Creek, Middle Mill Creek, Droxrock, Fallen Blocks and the Bunkhouse localities (Figures 2 and 3). Sections were photographed, sampled and logged for spectral gamma-ray measurements with a RS-125 scintillometer with 0.1–0.3 m vertical spacing. Sections were described in several field visits using an iterative approach in which detail from lithofacies characterization gathered from one visit and calibrated through subsequent petrographic work was integrated into observations made during subsequent visits. Palaeocurrent directions were measured from megaripples. The stratigraphic sections were correlated using distinctive lithofacies marker beds and signatures

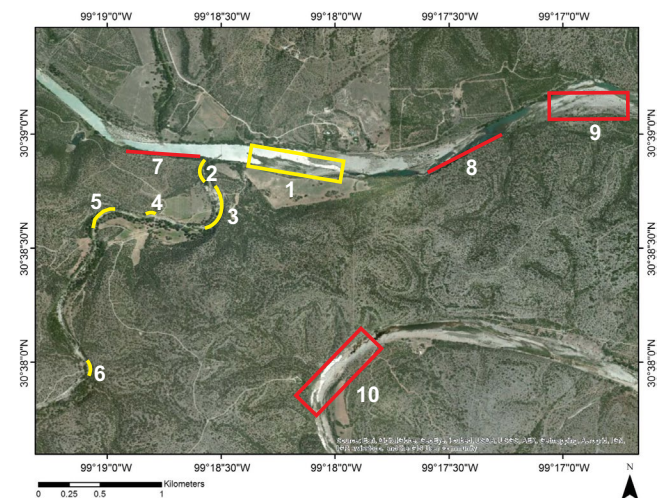


FIGURE 2 Satellite image of study area with localities of measured stratigraphic sections (yellow) and additional outcrops studied (red). Locality names are as follows: (1) Shepard Pavement, (2) Lower Mill Creek, (3) Mill Creek Cliff, (4) Droxrock, (5) Fallen Blocks, (6) Bunk House, (7) Shepard Cliff, (8) Zesch Cliff, (9) Zesch Pavement and (10) James River Pavement

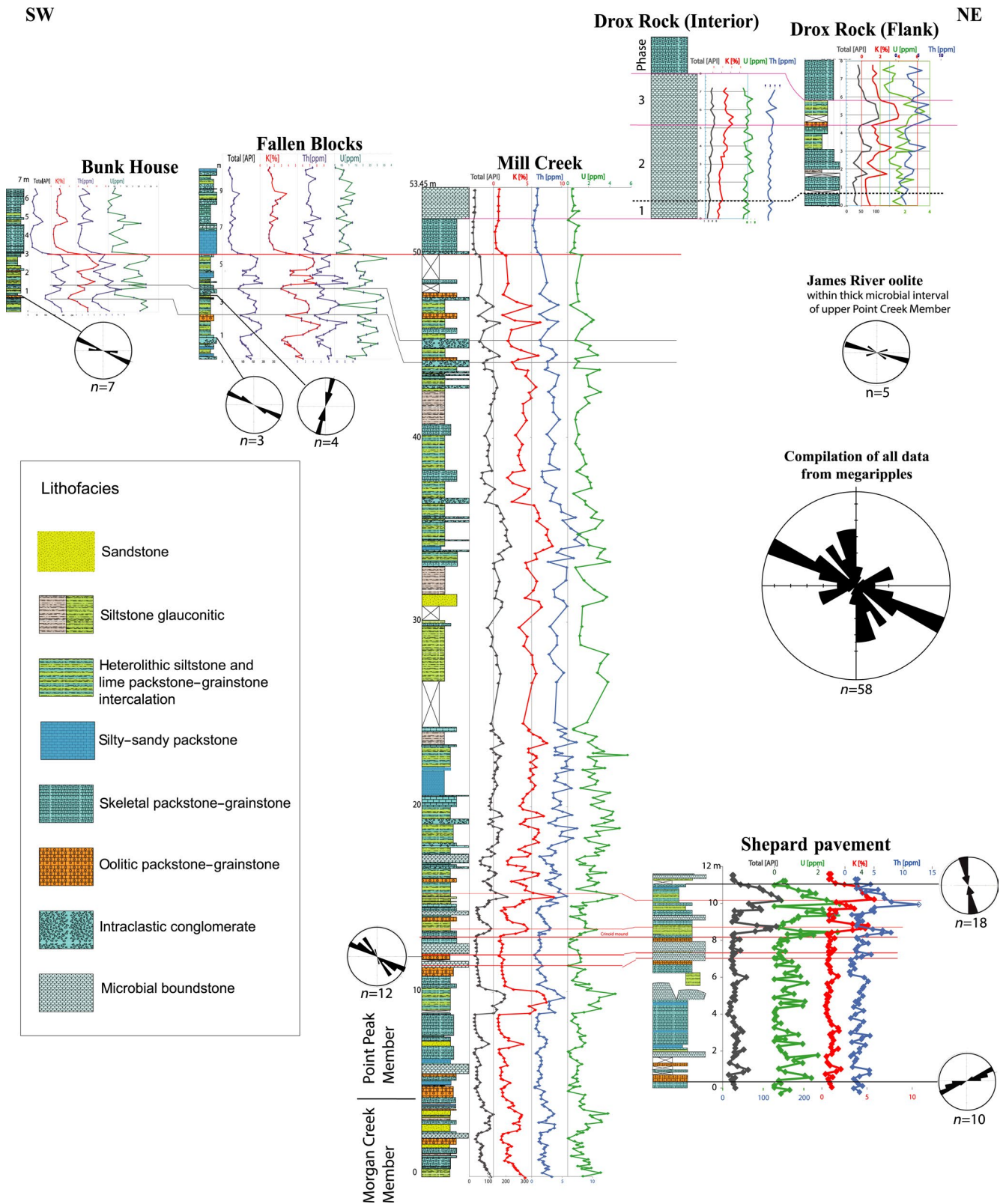


FIGURE 3 Detailed stratigraphic sections and correlations based on spectral gamma-ray curves and lithologic marker beds. Rose diagrams show azimuths of megaripple crests (perpendicular to direction of reversing flow) in skeletal and oolitic grainstone. Localities are shown in Figure 2

in gamma ray logs. Markov chain analysis of the composite stratigraphic section was performed using the techniques described in Lehrmann and Goldhammer (1999).

An aerial photography survey was conducted with a drone (quadcopter) equipped with a Sony NEX-7, 24.3 MP camera, gimble and a GPS. The images were georeferenced using

DGPS and total station surveys. Drone images of the Shepard and Zesch Pavements, Shepard, Zesch and Middle Mill Creek cliffs, Droxrock and Fallen Block localities (Figure 2) were used in this study to quantify macroscopic architectural features such as mound architecture and megaripples. Observations of the architecture of large microbial mounds in the upper Point Peak Member spectacularly exposed on the James River pavement were used to complement field observations from other sections.

Hand samples were used to make thin sections and polished slabs to document facies characteristics and smaller sedimentary structures. Drill cores (2.5 and 8 cm diameter and up to 60 cm long) were taken from a series of transects in Droxrock where lithofacies were difficult to systematically sample with a hammer. Numerous large blocks of entire microbial mounds, cross sections through megaripples and layers of flat-pebble conglomerate were collected and prepared as polished slabs to document larger scale structures. Polished slabs were imaged with a flat-bed scanner or digital camera. Slabs and thin sections were studied using a low-power binocular petrographic scope and a high-power petrographic scope. The nomenclature of Riding (2011) was used for description of microbial fabrics. Point counts were conducted using the grain-solid method (Flügel, 1982), with a variable number of points per sample (minimum of 100) depending on sample heterogeneity, using the program JMicroVision. A total of 248 polished slabs and 222 thin sections were analysed in this study.

4 | RESULTS

4.1 | Facies

Eight facies are recognized based on texture, composition, sedimentary structures, nature of stratigraphic contacts and bedding continuity (Table 1). Carbonate facies make up half of the stratigraphic thickness of the Mill Creek composite section (skeletal packstone to grainstone—16%, oolitic packstone to grainstone—5%, microbial boundstone—22% and intraclastic conglomerate—7%). The remaining half of the section thickness is composed of the mixed carbonate–siliciclastic heterolithic facies (21%) and siliciclastic sandstone and siltstone (29%; Table 2, Figure 3 and Figure S1). Volumetrically, carbonate depositional constituents (including all grain types, lime mud and marine carbonate-cement totalling 45.8%) comprise a slightly greater proportion than siliciclastic constituents (34.9%, Table 3).

4.1.1 | Fine to medium sandstone

Fine to medium sandstone is present in the uppermost Morgan Creek Member and basal Point Peak Member and within the

middle Point Peak Member at Mill Creek section (Figures 2 and 3). Sandstone beds are laterally continuous across outcrops and are friable and recessive making it difficult to determine details of the sedimentary structures. Where well exposed, sandstone is massive or horizontally laminated. The sandstone is composed of poorly sorted angular to subrounded grains of quartz, feldspar, mica, and in some cases, a trace of admixed glauconite pellets, skeletal or oolitic grains (Figure 4A). Intergranular space contains micrite matrix or equant calcite cement.

In the uppermost Morgan Creek and basal Point Peak members, sandstone is interbedded in sharp contact with sandy packstone–grainstone, skeletal packstone–grainstone and oolitic lime packstone–grainstone. In some cases, sandstone occurs in gradational contact with sandy lime-packstone to grainstone (Figure 3 and Figure S1). In the middle Point Peak Member, sandstone occurs within a thick recessive interval dominantly composed of siliciclastic siltstone (Figure 3 and Figure S1).

4.1.2 | Siltstone to very fine sandstone

Siltstone to very fine sandstone is the dominant siliciclastic facies and occurs as thin intercalations within the carbonate facies throughout the facies succession with the exception of the thick microbial mounds in the upper Point Peak Member (Figure 3 and Figure S1). It is also included as very thin intercalations within the heterolithic facies described below. The middle of the Point Peak Member is a recessive, relatively poorly exposed interval, dominantly composed of siltstone to very fine sandstone with thin subordinate carbonate intercalations (Figure 3 and Figure S1).

Siltstone to very fine sandstone beds weather recessively, have sharp contacts with intercalated facies, and are laterally continuous across outcrops except for localized areas where they onlap onto microbial mounds (see Discussion in microbial boundstone section below). An olive green colour in some intervals indicates the presence of disseminated glauconite. Siltstone to very fine sandstone is composed of angular quartz, feldspar and mica with a micritic carbonate matrix or microspar calcite cement (Figure 4B,C). The dominant sedimentary structure is horizontal lamination (Figure 4B). Extensively bioturbated, glauconite-rich intervals occur within the uppermost Morgan Creek and lower Point Peak members at the Shepard Pavement and Mill Creek sections (Figures 3, and 4D and Figure S1). Very fine sandstone intervals at 13.7, 14.5 and 15.8 m in the lower Point Peak Member at the Mill Creek section, associated with heterolithic, oolitic and microbial biostrome facies contain symmetrical ripples and interference ripples exposed on bedding surfaces (Figure 4E). The symmetrical ripples have wavelengths ranging from 2 to 7 cm (av. 5 cm) and heights of 0.5 to 0.6 cm (av. 0.55 cm).

TABLE 1 Facies characteristics and interpreted depositional environments

Facies	Characteristics	Thick (m)	Interpretation
Fine to medium sandstone	Laminated to massive, laterally continuous. Poorly sorted angular quartz, feldspar, mica. Micritic matrix or calcite cement. Trace of skeletal grains	Max. 0.62 Min. 0.07 Av. 0.3	Nearshore Facies Association Marine nearshore deposition, landward siliciclastic sediment source, increased delivery during regression
Siltstone to vf. sandstone, glauconitic	Laminated, symmetrical ripples or burrow mottled, laterally continuous. Angular quartz, feldspar, mica, glauconite	Max. 1.89 Min. 0.09 Av. 0.7	Marine nearshore, tidal flats, wave agitation, intertidal to shallow subtidal. Landward siliciclastic sediment source, possibly eolian, increased delivery during regression
Heterolithic flaser bedded siltstone-packstone	Dcm to cm intercalation of horizontally laminated siltstone and lenticular to continuous fine peloidal packstone. Ripple cross-lamination, reversing current indicators, scours, tidal bundling, desiccation cracks. Peloids, trilobites, echinoderms, angular quartz, glauconite	Max. 1.06 Min. 0.05 Av. 0.5	Intertidal tidal flat, flood and ebb tidal currents, intermittent subaerial exposure
Sandy-silty packstone to grainstone	Homogenous medium beds. Trilobite, eocrinoid and brachiopod fragments, peloids angular quartz, glauconite	Max. 1.56 Min. 0.09 Av. 0.3	Subtidal open marine, possibly homogenized by bioturbation
Skeletal packstone-grainstone	Laterally continuous, massive to cross-bedded, asymmetric megaripples with reversing current indicators. Lenses of dolomitized micrite. Reworked skeletal fragments with adhered micrite, gastropod steinkerns. Trilobite, eocrinoid and brachiopod fragments, peloids, ooids, glauconite pellets. Selective dolomitization of skeletal grains	Max. 1.8 Min. 0.1 Av. 0.38	Open-marine subtidal, tidal currents and storm wave agitation. Mud infiltrated into intergranular porosity during pauses in current agitation
Oolitic packstone-grainstone	Laterally continuous, massive to cross-bedded, asymmetric megaripples with reversing current indicators. Lenses of dolomitized micrite. Ooids with radial cortices, peloid or skeletal nuclei. Oolite lithoclasts. Grainstone extensively recrystallized, ooids commonly selectively dolomitized. Packstone with mud partly filling interparticle porosity, geopetals	Max. 0.46 Min. 0.16 Av. 0.28	Open-marine subtidal, tidal currents tidal currents and storm wave agitation. Mud infiltrated into intergranular porosity during pauses in current agitation
Intraclastic conglomerate	Broad lenticular channels several centimetre to decimetre deep and several metres across or laterally extensive sheets. Dominantly intercalated with heterolithic facies. Horizontal or imbricated clasts. Grainstone matrix. Rare edgewise rosette fabrics. Rounded flat-pebbles composed of heterolithic facies, and equant irregular, embayed, bored, micritized and oxidized clasts. Microbial clasts in breccia units shed from adjacent microbial mounds. Shrinkage cracks in oxidized clasts	Max. 0.49 Min. 0.05 Av. 0.18	Storm surge reworking of intertidal heterolithic sediment into broad channels and sheets on tidal flat. Transgressive lag at base of very thick bed of upper oolitic-skeletal microbial mound horizon

(Continues)

TABLE 1 (Continues)

Facies	Characteristics	Thick (m)	Interpretation
Microbial boundstone	<p>Biostromes composed of amalgamated round to complexly invaginated thrombolite and stromatolite mounds and small isolated mounds intertonguing with heterolithic facies or overlapped by siltstone in Lower Point Peak Mbr.</p> <p>Large complex mounds several metres tall by tens of metres wide composed of internal stromatolitic columns in Upper Point Peak Member. Growth stages include sharp-walled mounds with dense microbial rinds overlapped by siltstone or aggrading mounds intertongued with carbonate and siliciclastic intermound sediment. Substrates include flat-pebble conglomerate, hardgrounds and skeletal or oolitic grainstone. Clotted microbial micrite, <i>Girvanella</i>, <i>Tarthinia</i>. Entrapped trilobite, eocrinoid and brachiopod fragments. Entrapped siliciclastic silt and sand in microbialities of Lower Point Peak Mbr</p>	<p>Max. 7.7^a</p> <p>Min. 0.21</p> <p>Av. 1.45</p>	<p>Biostromes and small mounds in Lower Point Peak Member interpreted to be intertidal by association with intertonguing heterolithic facies. Entrapped siliciclastic sediment indicates growth during flux of siliciclastics onto the tidal flat. Large complex mounds of Upper Point Peak are interpreted to represent open-marine offshore environments</p>

^aThickness at Droxtrock on Mill Creek composite section.

4.1.3 | Heterolithic flaser-bedded siltstone–packstone

Heterolithic, flaser-bedded siltstone–packstone is a mixed carbonate–siliciclastic facies that occurs throughout the upper Morgan Creek and Point Peak members intercalated with carbonate facies (Figure 3 and Figure S1). The facies is moderately recessive, but exceptionally well-exposed in cliff sections (Figure 5A). The heterolithic facies is thin bedded and typically laterally continuous across outcrops except for areas where intervals contain interspersed microbial mounds.

The heterolithic facies is composed of centimetre-scale to decimetre-scale intercalations of horizontally laminated siltstone and lenticular to continuous, very fine grained peloidal and skeletal carbonate packstone (Figure 6A). The siltstone is identical to the facies described above; it ranges from tan or olive green in colour indicating the variable presence of disseminated glauconite. Packstone interbeds are composed of very fine sand-sized peloids and trilobite fragments, echinoderm debris, angular quartz silt and glauconite.

Packstone interbeds are lenticular to continuous. The lenticular structure results from asymmetric ripple forms, and starved asymmetric ripples, with scour structures and reversing current indicators (Figure 6A,B). Rippled intervals are draped by siltstone. The base of the carbonate interbeds is commonly sharp and planar, and may be formed of scoured surfaces that truncate laminae in the underlying siltstone. Intervals a few centimetres thick contain bundles of thickening and thinning muddy/grainy carbonate and silt lamination that are interpreted to be tidal bundles (Figure 6C,D; Tape *et al.*, 2003). V-shaped cracks in the upper part of carbonate beds or carbonate-rich siltstone were observed in vertical cross sections (Figure 6A,C) within the heterolithic facies in the carbonate-rich portion of the lower Point Peak (Mill Creek section, 13–20 m) and below the upper microbial horizon in the upper Point Peak (Mill Creek section, 44–48 m, Fallen Blocks section, 1.3–5.5 m; Figure 3 and Figure S1). In cross section, the cracks are regularly spaced laterally, have a V-shaped morphology that penetrates downward into the bed and are infilled by overlying sediment (Figure 6A,C). Identical features were observed in bedding-plane exposures where they form polygonal cracks in heterolithic facies below the upper microbial horizon in the upper Point Peak at the Zesch Cliff Locality (Figure 6E). These features are interpreted to be desiccation cracks.

4.1.4 | Sandy or silty packstone to grainstone

Sandy to silty skeletal packstone to grainstone is a minor component of the stratigraphic section (Figure 3 and Figure S1). It is identical to the skeletal packstone to grainstone

TABLE 2 Compositions of carbonate and mixed carbonate-siliciclastic facies

Carbonate and mixed carbonate-siliciclastic facies	Microbial boundstone	Skeletal packstone to grainstone	Oolitic packstone to grainstone	Intraclastic conglomerate	Heterolithic
Facies thickness % of section ^a	22	16	5	7	21
Constituent	Composition % from point counts				
Trilobite		12	5	6	1
Eocrinoid		12	10	3	1
Brachiopod		5			1
Gastropod		1			
Unidentified skeletal		4			
Ooid		2	39	1	
Peloid	1	3	5	5	20
Intraclast (heterolithic)		1		23	
Intraclast (micrite)		3	4	20	
Intraclast (microbial)				2	
Lime mud (micrite)	22	17	9	18	15
Equant spar	9	10	14	4	18
Bladed cement		6	1		
Syntaxial cement overgrowth			1		
Dolomite	13	9	4	6	2
Clotted microbial micrite	51				
Calcmicrobial framework	1				
Quartz silt sand	2	3		6	34
Mica				1	6
Glauconite	1	13	5	5	2

^aSiliciclastic sandstone and siltstone make up 29% of total section thickness.

facies described below except that it contains admixed quartz sand or silt.

4.1.5 | Skeletal packstone to grainstone

Skeletal packstone to grainstone forms prominent resistant beds, laterally continuous across outcrops, within the carbonate-dominated portion of the section in the upper Morgan Creek–lower Point Peak and in the upper Point Peak (Figure 3 and Figure S1). Skeletal packstone to grainstone beds may be massive bedded, burrow mottled or contain cross-bedding and asymmetric megaripples. Prominent asymmetric megaripples and cross-bedding are well preserved at several levels in the upper Morgan Creek and lower Point Peak members in the Mill Creek, Fallen Blocks and Shepard Pavement sections (Figure 3, Figure S1, Figures 5A,B and 7A,B). Rippled and cross-bedded intervals contain occasional lenses of dolomitized micrite sometimes occurring in the troughs of cross-beds or between megaripples. The megaripples contain evidence of reversing current directions with the cross-laminae facing different directions separated by reactivation surfaces. Megaripples have wavelengths ranging from 70 to

82 cm (av. 76 cm) and amplitudes from 4 to 8 cm. Stoss slope angles range from 8 to 16° (av. 13°) and lee slope angles are 18–24° (av. 20°). Azimuth data are shown in Figure 3. Azimuth of ripple crests (perpendicular to current flow) in the Point Peak at the Mill Creek and Shepard Pavement sections average 129°–309° (13.2 m Mill Creek section), 168°–348° (10.9 m Shepard Pavement section) and 120°–300° (1.17 m Fallen Blocks section).

Skeletal packstone to grainstone is composed of fragments of trilobite sclerites and eocrinoid ossicles with lesser gastropod and brachiopod fragments, peloids, glauconite pellets and rare ooids (Figure 7C,D). Skeletal material is entirely fragmental and commonly broken and rounded (Figure 7C,E), with the most complete skeletal components being rare eocrinoid hold-fasts on hardgrounds, and concentrations of disarticulated brachiopods found on bedding planes and in the troughs between megaripples in the lower Point Peak Member. Trilobite fragments are reworked clasts with adhered micrite preserved in protected inner curves “shepherd crooks” of the shell (Figure 7D). Likewise, gastropods are preserved as reworked steinkerns (Figure 7D).

Skeletal beds are dominantly grainstone. Packstone contains lime mud in crude laminae or burrow mottles within

TABLE 3 Total volumetric contribution of constituents to total volume of section^a

Constituent class	% vol. ^a	Constituent class	% vol. ^a
Non-skeletal grains		Microbial	
Peloid	5.6	Clotted-massive micrite	11
Ooid	2.4	Intraclast microbial	0.2
Intraclast (heterolithic facies)	1.7	Calcimicrobial framework	0.4
Intraclast (micrite)	1.9	Encrusting micrite	0.1
Total non-skeletal grains	11.6	Total microbial	11.7
Micrite		Marine cements	
Lime mud (micrite)	13.8	Bladed cement	1
Total micrite	13.8	Syntaxial cement overgrowth	0.1
		Total marine cement	1.1
Skeletal		Total depositional carbonate (including marine cement)	
Trilobite	2.9		45.8
Eocrinoid	2.2		
Brachiopod	1.7		
Gastropod	0.2	Siliciclastic grains	
Unidentified skeletal	0.6	Quartz and feldspar silt and sand	28.4
Total skeletal carbonate	7.6	Mica	3.1
		Glauconite	3.4
		Total siliciclastic	34.9
		Late diagenetic	
		Equant spar	14.6
		Dolomite	5.4
		Total late diagenetic	20

Note: Proportions of carbonate/heterolithic/and siliciclastic facies change through transgressive–regressive cycles (Figure 15). During transgressive phase facies proportions range to 67% carbonate, 23% heterolithic and 10% siliciclastic whereas during regressive phase facies proportions range to 16% carbonate, 23% heterolithic and 61% siliciclastic.

^aVolumetric estimates are based on weighting of point count measurements of samples by thickness proportion of facies in the Mill Creek composite section as follows: medium to fine sandstone (3.4%), very fine sandstone to siltstone (25.9%) heterolithic (20.9%), microbial (21.6%), intraclastic (6.7%), skeletal (16.3), oolitic (5.3%).

dominantly grainy sediment or as mud infiltrated into intergranular porosity (Figure 7C). Isopachous-bladed cement and poikilotopic calcite spar on skeletal grains is followed by equant calcite spar infilling interparticle porosity (Figure 7C,E). Skeletal grains are commonly selectively

dolomitized. Skeletal packstone to grainstone beds are dominantly of medium bed thickness (av. 0.38 m) with the exception of a few thick beds in the carbonate-rich lower portion of the Point Peak and a very thick bed of skeletal–oolitic grainstone (1.8 m thick) adjacent to and at the base of the thick microbial mound horizon in the upper Point Peak (Mill Creek section 51.7–53.5 m, Figures 3, 8A and 9A). The base of this bed is important as it marks an abrupt shift from siliciclastic-dominated sedimentation below to microbial and oolitic carbonate-dominated sedimentation above. The bed is continuous across the field area but contains a variable proportion of skeletal vs. ooid content. In sections at Mill Creek, the bed is dominantly bioclastic with a conspicuous proportion of ooids, whereas in the James River pavement it is dominantly oolitic (Figure 2).

4.1.6 | Oolitic packstone to grainstone

Oolitic packstone to grainstone forms prominent resistant beds, laterally continuous across outcrops, within the carbonate-dominated portion of the section in the upper Morgan Creek–lower Point Peak and in the upper Point Peak (Figure 3 and Figure S1). Beds are most commonly thin to thick bedded except for the very thick bed of skeletal–oolitic grainstone at the base of the thick microbial mound horizon in the upper Point Peak Member (Figures 3, 8A and 9A). Oolitic beds are stratigraphically associated with skeletal packstone–grainstone and microbial boundstone (Table 1, Figure 3 and Figure S1). At three stratigraphic levels in the lower and upper Point Peak, megaripped oolitic grainstone sharply overlies flat-pebble intraclastic conglomerate (Figure 10A,B and Figure S1). The very thick bed of skeletal–oolitic grainstone at the base of the thick microbial mound horizon occurs laterally adjacent to and underlying the lower part of microbial buildups (Figure 9A).

Sedimentary structures include cross-bedding and asymmetric megariipples and lenses of dolomitized micrite, sometimes occurring in the troughs between megariipples. The megariipples contain evidence of reversing current directions (Figure 10A,B). Megariipples have wavelengths ranging from 74 to 150 cm (av. 107 cm) and amplitudes from 6 to 10 cm. Stoss slope angles range from 7 to 15° (av. 12°) and lee slope angles 10–21° (av. 16°). Azimuth data are shown in Figure 3. Azimuth of ripple crests in the lower Point Peak average 73°–253° (0.6 m Shepard Pavement) and in the upper Point Peak average 17°–197° (3.4 m Fallen Blocks section) and 111°–291° (0.89 m Bunk House section). Measurements of megariipples at the James River pavement (Figures 2 and 3), within oolite immediately below and within the very thick bed of skeletal–oolitic grainstone at base of the thick microbial mound horizon in the upper Point Peak, have wavelengths in

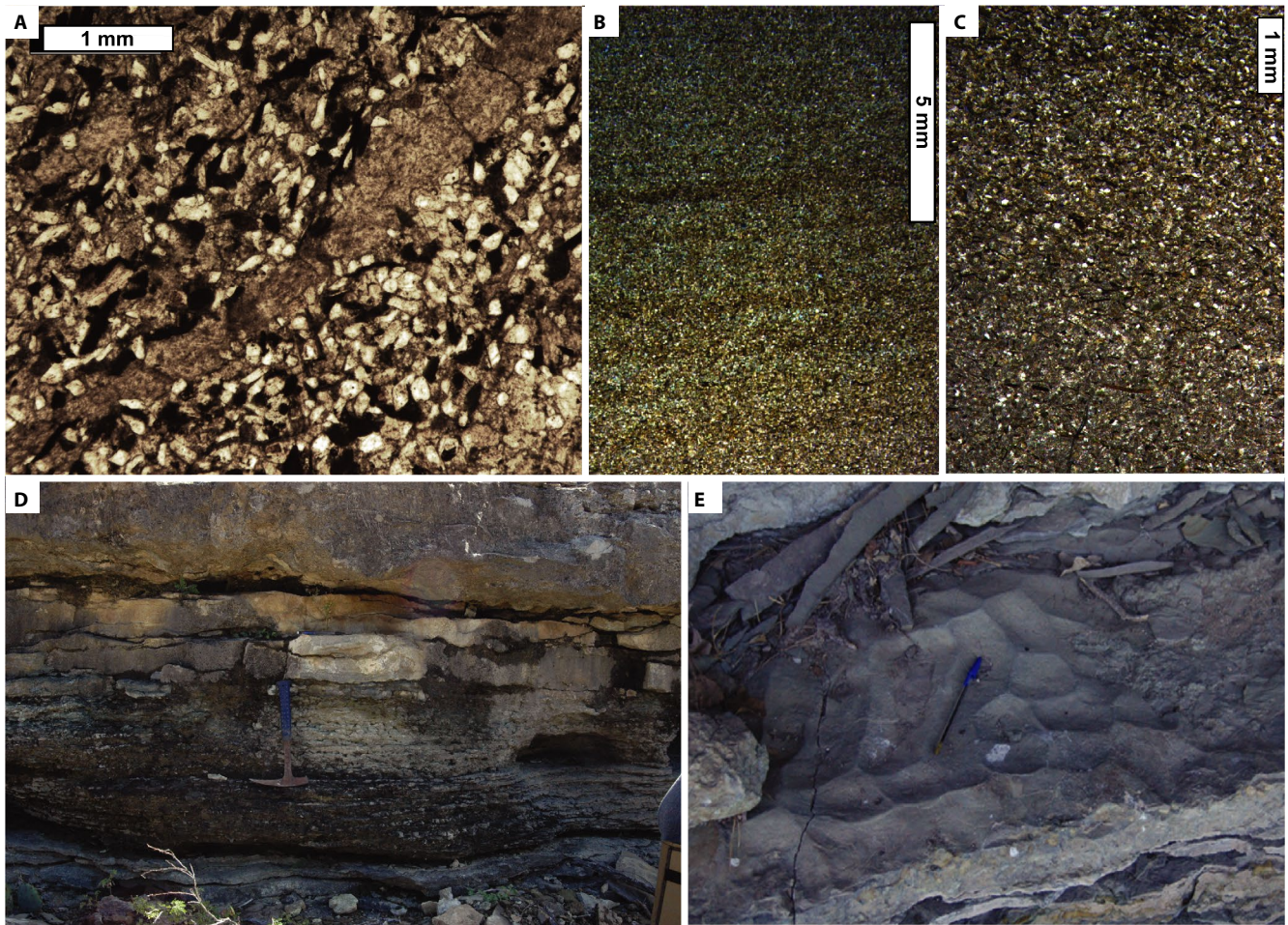


FIGURE 4 Sandstone and siltstone facies. (A) Medium sandstone with glauconite pellets and carbonate mud layers. Thin-section, plane-polarized light. Mill Creek Section, 1.6 m. (B) Planar-laminated very fine sandstone. Thin-section, cross-polarized light. Fallen Blocks Section, 1.18 m. (C) Siltstone, containing angular quartz grains, mica and carbonate mud matrix. Thin-section, cross-polarized light. Mill Creek Section, 16.4 m. (D) Bioturbated glauconitic siltstone. Outcrop. Hammer is 33 cm. Mill Creek Section, 13.4 m. (E) Very fine sandstone with symmetrical interference ripples. Outcrop. Pen is 14 cm. Mill Creek Section, 16.9 m

the studied sections ranging from 54 to 130 cm (av. 84 cm) and amplitudes from 4 to 8 cm. Stoss slope angles range from 10 to 21° (av. 16°) and lee slope angles 17–28° (av. 23°). Azimuths of ripple crests average 106°–286° (Figure 3).

Megaripples and cross-bedded intervals are grainstone, whereas massive beds may be packstone. Oolitic grainstone in the lower part of the Point Peak Member at the Mill Creek and Shepard Pavement sections contains composite coated grains and rounded, pebble sized, oolite lithoclasts (Figure 10A). Oolitic grainstone is typically strongly recrystallized or pervasively dolomitized with ooids preserved as ghost fabrics (Figure 10C). Oolitic packstone contains micrite and peloidal sediment that infiltrated into intergranular pores (Figure 10D,E). Fabric details are better preserved in packstone. Ooids contain peloid or skeletal grain nuclei and radial cortical fabric, outer margins may be micritized (Figure 10D,E). No quartz nuclei were observed in any of the samples. Ooids are commonly preferentially dolomitized. Ooids range from 0.5 to 2.2 mm in size, very few grains

exceed 2 mm. Oolitic packstone and grainstone may contain admixed trilobite, echinoderm and brachiopod fragments, and lesser rounded intraclasts, peloids and glauconite pellets. A quartz sand component was found only within oolite beds of the upper Morgan Creek Member at the base of Mill Creek section (Figure 3 and Figure S1).

4.1.7 | Intraclastic conglomerate

Intraclastic conglomerate occurs in thin to medium lenticular channelized beds or sheets that are laterally continuous across outcrops (several tens of metres), dominantly intercalated with heterolithic facies with sharp or erosive contacts, and also commonly underlie microbial boundstone mounds and bios-tromes and oolitic grainstone–packstone beds (Figures 3, 8, 9A and Figure S1). A layer of intraclastic conglomerate occurs at the base of the very thick bed of skeletal oolitic packstone–grainstone that forms the substrate of large microbial

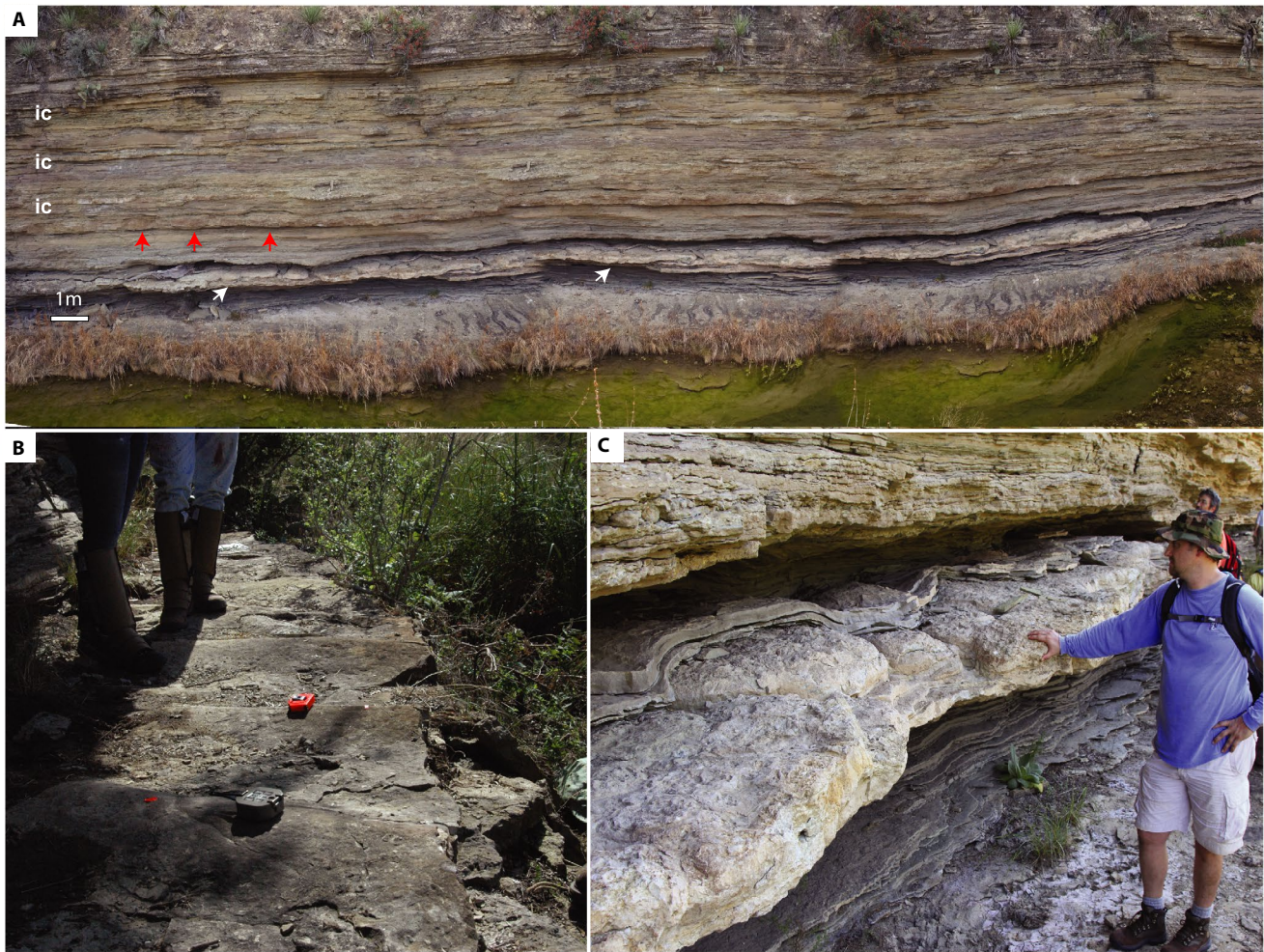


FIGURE 5 Overview of Mill Creek Cliff exposure. (A) Drone image of the lower portion of Mill Creek cliff. Approximately 7 m of vertical section shown (12–19 m in Mill Creek Section (Figure 3 and Figure S1)). Megaripped oolitic grainstone lower, microbial biostrome (white arrows) and isolated mounds (red arrows) intertongued with heterolithic facies and change laterally to right into continuous biostrome. Lenticular and continuous layers of intraclastic conglomerates (ic) intercalated with heterolithic facies. (B) Megaripped oolitic grainstone. Same unit as shown in base of (A), 12 m in Mill Creek Section (Figure 3 and Figure S1). (C) Coalesced microbial mounds forming biostrome. Same unit as near bottom of section in (A), 13.9 m in Mill Creek Section (Figure 3 and Figure S1)

mounds in the upper Point Peak Member (Mill Creek section 51.7–53.5 m; Figures 3, 8A and 9A). Flat-pebble conglomerates are not found within the microbial mounds and associated facies in the upper Point Peak strata above this level (Figure 3). Channel forms are broad, flat-based features, approximately 5–15 m across with concave-up margins up to 30 cm deep. The channels truncate underlying heterolithic strata and have flat tops (Figures 8 and 9A). The channel margins are usually not smooth, but rather step-like, where flat pebbles were plucked from the intervening thinly layered heterolithic sediment.

In the Mill Creek section, two fundamentally different clast types are observed, often segregated into different intraclastic beds, although occasionally they may be mixed. Dominant clasts are rounded to subangular, flat pebbles composed of the heterolithic facies (Figure 11A,B). The subordinate clasts are strongly micritized, oxidized and equant, with highly irregular,

embayed margins (Figure 11C,D). Petrographic observations indicate that micritized clasts contain micritization fronts that only partially replaced clasts; the preserved component is skeletal material similar to the skeletal packstone–grainstone facies (Figure 11E). The oxidation is likely oxidized glauconite that had mineralized the material making up the clasts. Irregular embayments may be dissolution features, whereas regular circular embayments are likely to be borings (Figure 11C). Margins and interiors of the micritized clasts also contain peculiar V-shaped tensional cracks that appear to have resulted from shrinkage during diagenesis (Figure 11F). The matrix of intraclastic conglomerate is skeletal grainstone containing trilobite, eocrinoid and brachiopod fragments, peloids, quartz silt and glauconite pellets (Figure 11B).

Flat pebbles are commonly oriented subhorizontally, crudely imbricated (Figure 11A,B) and are occasionally found with

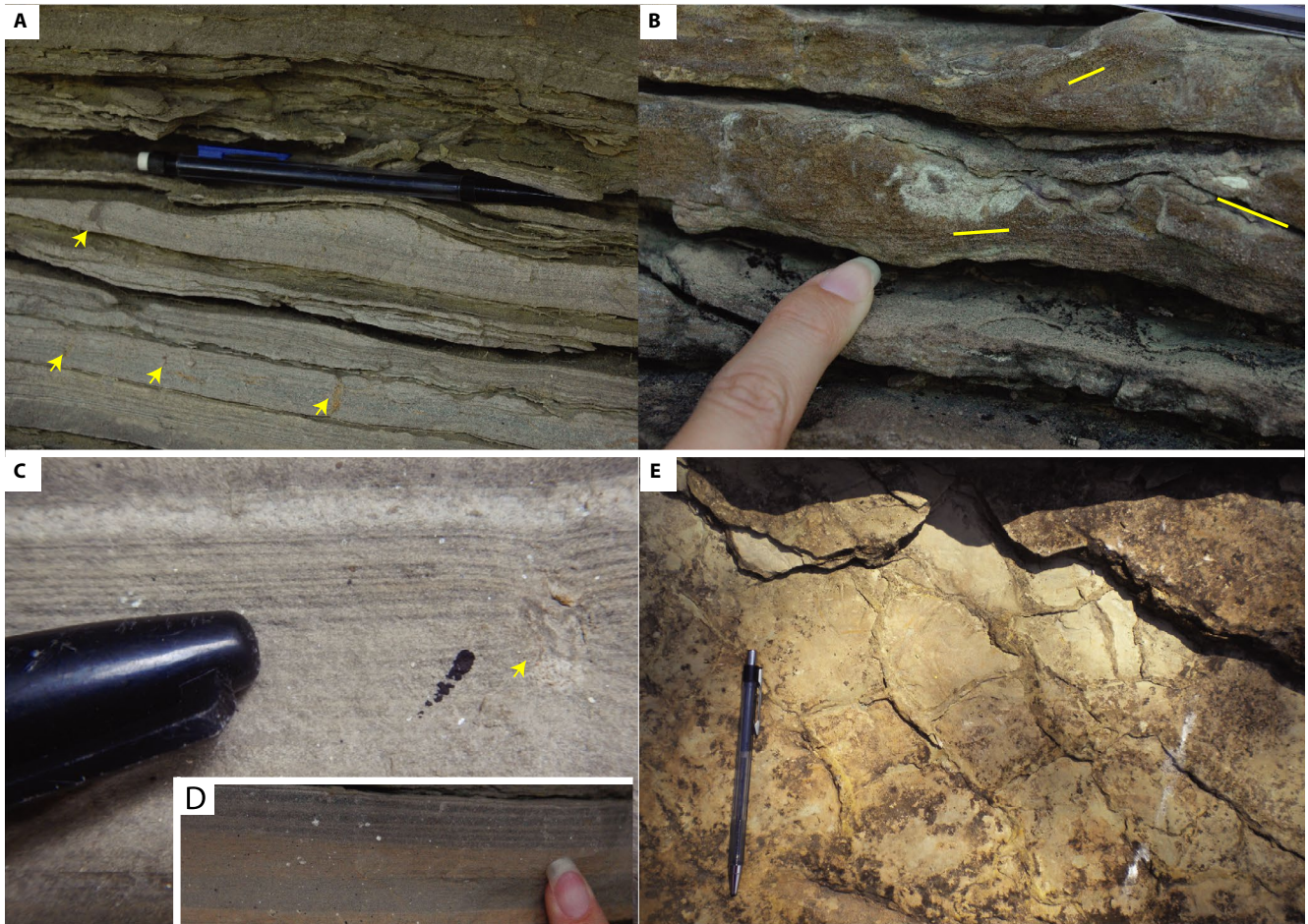


FIGURE 6 Heterolithic facies outcrop photos. (A) Flaser-bedded intercalation of carbonate peloidal packstone and siltstone layers. Isolated asymmetric ripples (below pen), desiccation cracks (arrows). Pen is 14 cm. (B) Flaser-bedded intercalation of carbonate peloidal packstone and siltstone layers. Ripple forms with reversing current indicators (lines). Mill Creek Section, 16.3 m. (C) Carbonate bed in heterolithic facies with alternating silt-carbonate mud laminae forming tidal bundle (left above pen cap) and desiccation crack (right). Fallen Blocks Section, 4.32 m. Pen cap for scale is 1.5 cm in diameter. (D) Tidal bundle composed of thickening to thinning package of silt-carbonate mud laminae. Mill Creek Section, 15.5 m. (E) Desiccation cracks on bedding plane view in heterolithic facies in upper Point Peak Member several metres below the large microbial mounds at Zesch Cliff. Pen is 14 cm

spar-filled shelter pores beneath flat pebbles (Figure 11D). In the lower Point Peak at the Mill Creek section (17 m) flat-pebble conglomerates locally have vertical “edge wise” orientations where they are stacked up adjacent to microbial mounds. In the upper Point Peak in the interval a few metres below the upper, thick microbial mound horizon at the Zesch Pavement and below the Zesch Cliffs, a few layers dubbed “pin-wheel conglomerates” by Ahr (1967) have vertically oriented clasts with highly organized, imbricated and radially distributed domains (rosette fabric; Demicco and Hardie, 1995, their fig. 27).

4.1.8 | Microbial boundstone

Microbial boundstone occurs within carbonate-rich portions of the section in the upper Morgan Creek and lower Point Peak members as several thin intervals of mounds and

biostromes (0.2–0.8 m thick; Figures 3 and 5), and as thick, large complex mounds in the upper Point Peak (7.7 m thick at Droxxrock, Mill Creek section, up to 14 m thick in cliffs along Llano River; Figures 3 and 9A.; Khanna *et al.*, 2019). Microbial boundstone is associated with oolitic and skeletal packstone–grainstone facies (Table 1, Figure 3 and Figure S1).

Microbial intervals of the upper Morgan Creek and lower Point Peak members consist of small isolated mounds (typically less than one metre across) and laterally extensive biostromes (Figures 5A and 12A,B). Biostromes are composed of coalesced oval to circular mounds (Figure 5A,C). Coalesced mounds in biostromes also form elongate and fitted fabric where mounds develop straight, concave or nearly polygonal shapes by interference of growth against adjacent mounds (Figure 12C). Individual mounds are separated by inter-mound detrital carbonate or heterolithic facies and change

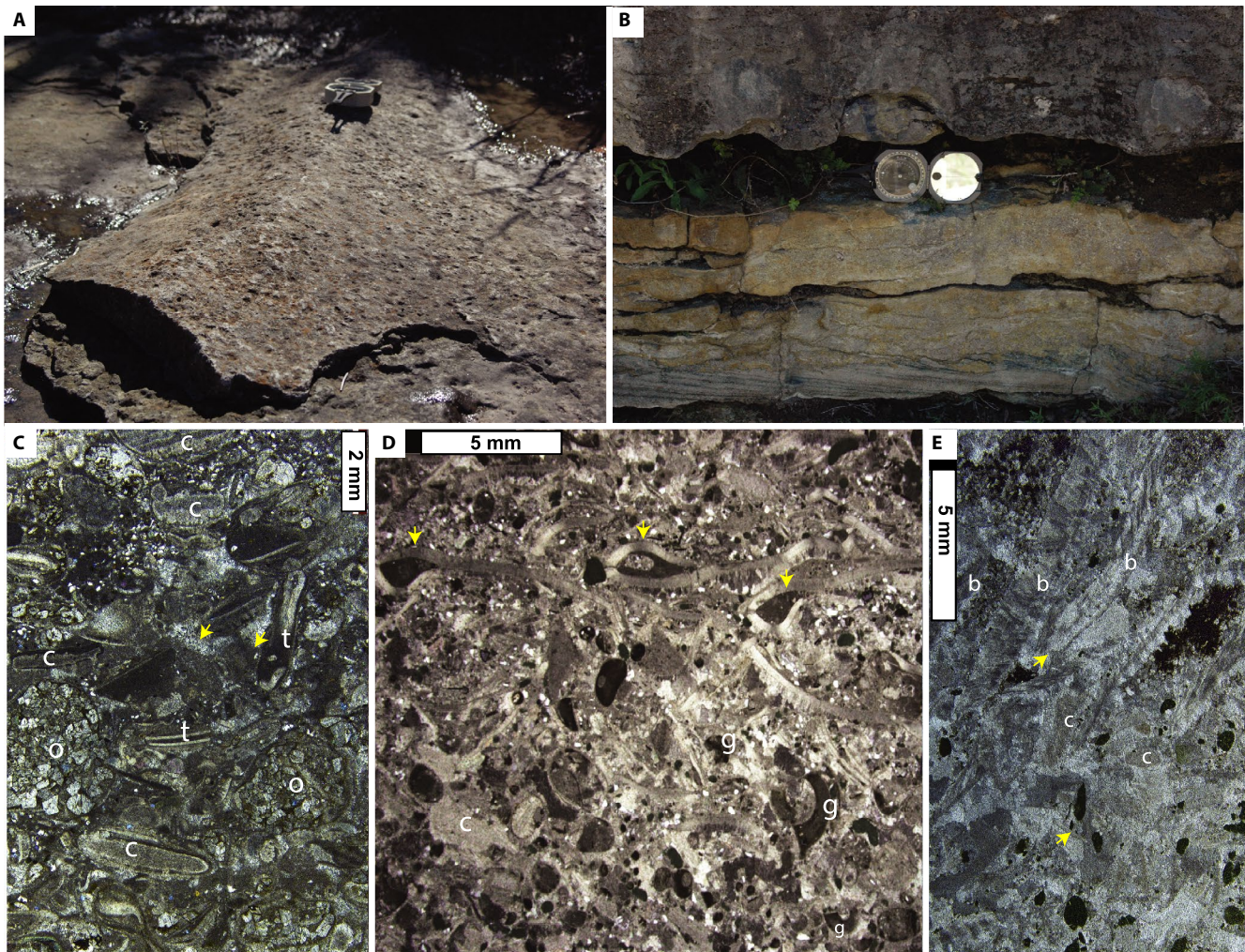


FIGURE 7 Skeletal packstone to grainstone. (A) Outcrop of asymmetric megaripple in skeletal grainstone. Brunton compass for scale. Shepard Pavement Section, 10.9 m. (B) Cross-bedded bioclastic skeletal grainstone. Brunton compass for scale. Mill Creek Section, 13.0 m. (C) Silty skeletal packstone with eocrinoid ossicles [c], oomoulds [o], trilobite fragments [t] and lime mud infiltrated into intergranular pores [arrows]. Skeletal grains are broken and rounded. Thin-section, cross-polarized light. Shepard Pavement Section, 4.6 m. (D) Silty skeletal grainstone with abundant trilobite fragments with lime mud adhered to protected “shepherd’s crook” area of skeletal fragments (arrows), gastropod steinkerns [g], eocrinoid ossicles [c], glauconite pellets (dark grains) and angular quartz silt. Thin-section, cross-polarized light. Shepard Pavement Section, 3.0 m. (E) Skeletal grainstone composed of disarticulated and broken articulate brachiopods [b] and eocrinoid ossicles [c]. Arrows indicate broken end of shell and shell fragments. Bladed marine-cement fringes on grains. Thin-section, plane-polarized light. Up is to the left. Shepard Pavement Section, 2.1 m

laterally over tens of metres into biostromes composed of coalesced mounds (Figure 5A). Mounds within biostromes occur as circular or oval thrombolite structures and complexly infolded (invaginated) “meandroid” thrombolites that commonly contain a dense micritic leolitic or stromatolitic rind (Figures 5A,C and 12D,E). Thrombolite clots are one to a few centimetres across (Figure 12D,E). Detrital sediment in the passages between mounds and “meandroid” structures in the biostromes of the lower Point Peak contain intercalated layers of skeletal–oolitic grainstone, carbonate mud and siliciclastic silt.

Isolated mounds in the lower Mill Creek section are nucleated on flat-pebble intraclastic conglomerate, have columnar to upward expanding morphology and have flanks that inter-tongue with intermound heterolithic facies (Figure 12A,B).

Sharp-walled, isolated mounds have dome to flat-topped shapes, circular to elongate shape in plan-view and occur one to several metres apart or locally coalescing in the Shepard Pavement section from 4.7 to 5.6 m (Figure 13A). The sharp-walled mounds range from 0.3 to 3.5 m across and are 0.4 to 0.9 m in height. The mounds are nucleated on an extensive skeletal–grainstone hardground pavement with adhered eocrinoid holdfasts (Figure 13A,B). Early lithification of the hardground is indicated by isopachous-bladed marine cement. The mounds are overlapped and draped by siliciclastic siltstone that has been mostly stripped away by erosion.

Internal structures of bioherms and mounds in the lower Point Peak Member include thrombolitic mound interiors that are commonly partially dolomitized and dense undolomitized micritic leolitic or stromatolitic external rinds.

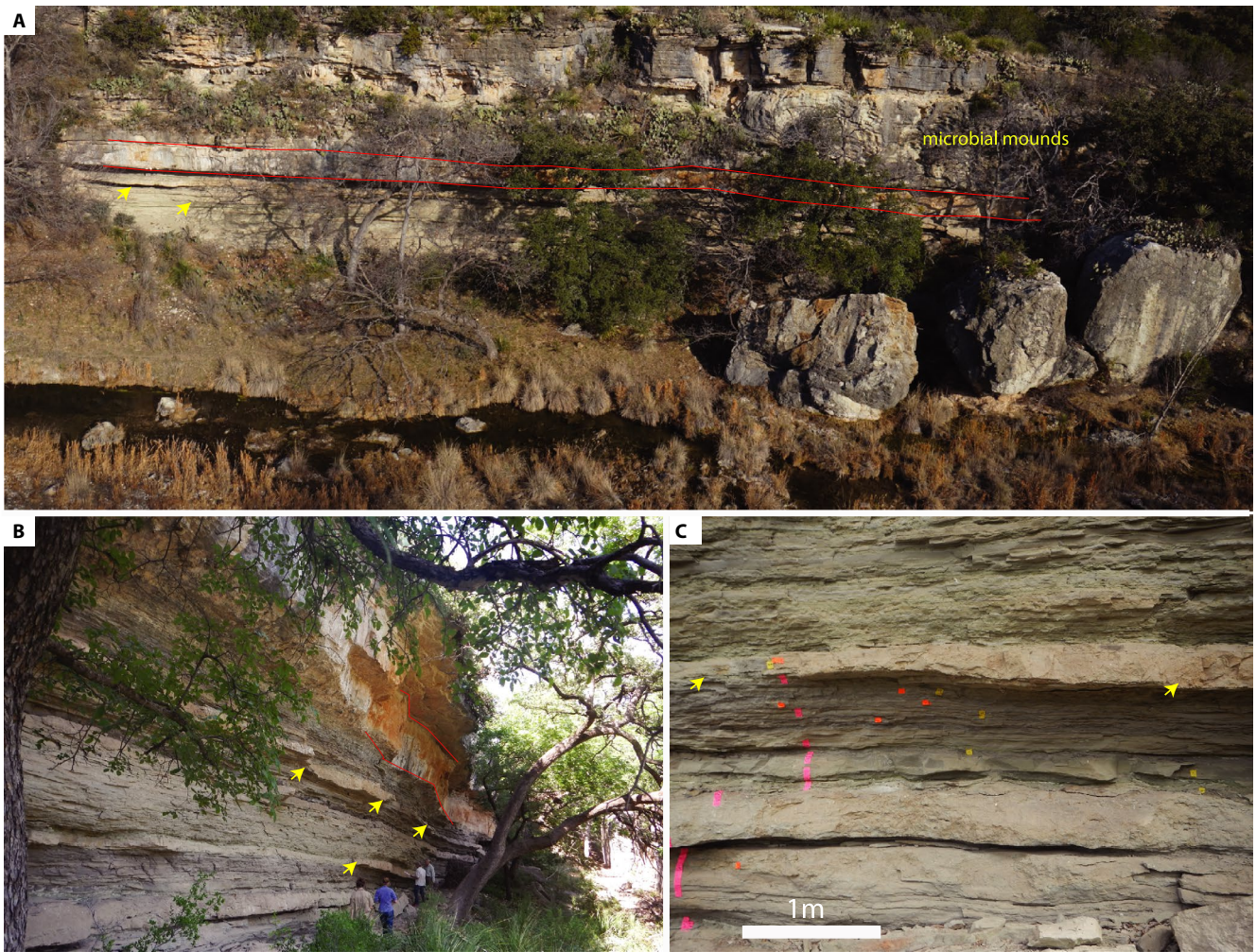


FIGURE 8 Overview of Fallen Blocks exposure. (A) Drone image. From the base of the cliff to the bottom of the massive microbial mound interval, the stratigraphic section is approximately 5.5 m thick. Lenticular channel fills of intraclastic conglomerate intercalated with heterolithic facies (yellow arrows) and very thick bed of skeletal–oolitic grainstone (highlighted with red lines) just below the level of the thick microbial interval. (B) Closeup oblique view of same exposure as shown in (A) view to north-east. Lenticular channel fills of intraclastic conglomerate intercalated with heterolithic facies (yellow arrows) and very thick bed of skeletal–oolitic grainstone (highlighted with red lines). People for scale. (C) Lens of intraclastic conglomerate intercalated with heterolithic facies (arrows)

Thrombolitic structures are composed of cauliflower or irregular lobate clots of dense or peloidal microbial micrite with intervening entrapped detrital carbonate and siliciclastic silt (Figure 12E,F). Entrapped detrital carbonate allochems include trilobite and eocrinoid fragments and ooids (Figure 12F). Within the complex invaginated “meandroid” biostromes microbial micrite shrubs progressively coalesce towards the outer surface of the structure forming a dense micritic rind (Figure 12E).

Microbialites in the upper Point Peak Member are composed of the large complex mounds prominent in the cliffs along the Llano River (Figure 9A) and accessible for detailed study in the outcrops along Mill Creek and James River (Figure 2). Outcrops in the Fallen Blocks section and drill cores from James River demonstrate that the large microbial mounds developed on a flat-pebble conglomerate layer that also occurs at the base of the very thick and laterally

extensive bed of skeletal–oolitic grainstone that formed at the same level and adjacent to the base of the large mounds (Figures 8A and 9A; Khanna *et al.*, 2019).

Analysis of drone images and ground observations of the James River pavement by Khanna *et al.* (2019) demonstrates that the microbial buildups in the upper Point Peak consist of several scales of macroscopic stromatolitic structures encapsulated in decimetre to metre-thick, dense micritic and finely clotted thrombolitic rinds that are nested to comprise larger buildups. These include decimetre-scale stromatolitic columns that are clustered into metre-sized intermediate-scale mounds (Figures 9B and 13C), that are grouped into yet larger mounds tens of metres across, and finally, mound complexes hundreds of metres across (Khanna *et al.*, 2019). Intermediate to large-scale mounds exposed in the James River and Zesch pavements display plan-view shapes ranging from oval to circular (e.g. Figure 9B). Analysis of drone

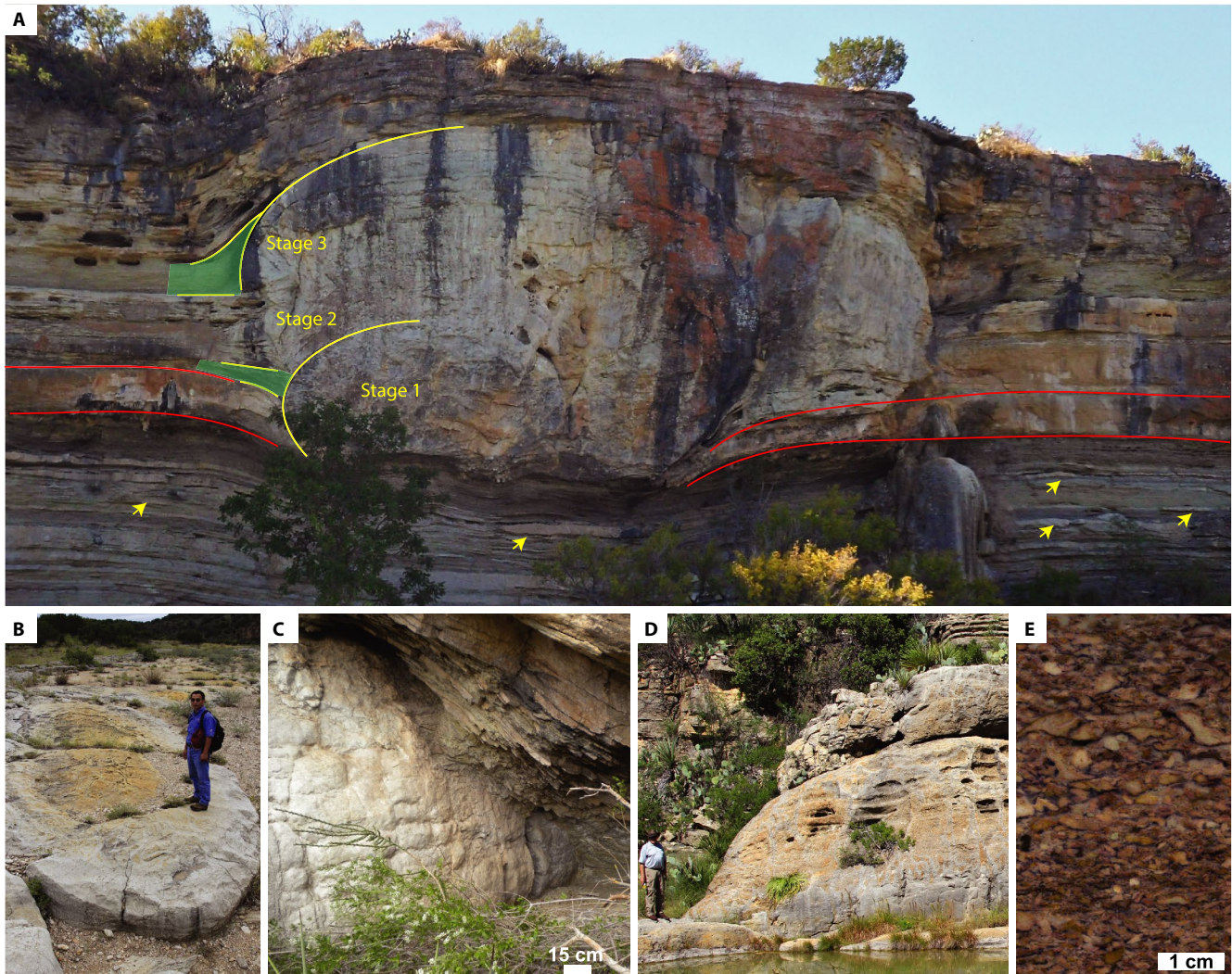


FIGURE 9 Overview of microbialite structures in the interval of large microbial mounds developed in the upper Point Peak Member. (A) Drone image of large microbial mound on the Shepard Cliff exposure on the Llano River (Whites Crossing area). Interpretation of 3 phase evolution with sharp-walled phases 1 and 3 overlapped by intermound siltstone facies (shaded green) separated by phase 2 which intertongues with detrital carbonate and siliciclastic intermound facies. (B) Elongated intermediate size mound with dolomitized interior (orange colour) containing decimetre-scale stromatolite columns surrounded by dense undolomitized-micritic rind. Mound is elongated in NE-SW direction. James River Pavement. (C) Dense micritic rind and sharp outer wall of phase 3 mound (left) overlapped by siliciclastic silt (right). James River Pavement. (D) Droxrock mound on Mill Creek. Dolomitized vertical stromatolite columns (orange colour) are evident in the interior of phase 2. Person for scale. (E) Microbial-clast intraclastic grainstone shed from phase 2 mound and intertonguing with intermound detrital facies. Angular dense micritic microbial clasts. Polished slab. Fallen Blocks Section, 7.09 m

images by Khanna *et al.* (2019) demonstrates that elongate intermediate to large-scale mounds and complexes within the James River pavement have a dominant NE-SW orientation.

Khanna *et al.* (2019) demonstrated that large microbial mounds in the upper Point Peak Member contain a three-phase architecture including lower and upper buildup phases (phases 1 and 3) with a dense micritic and finely clotted thrombolitic rind and sharp outer wall of the mound overlapped by siliciclastic siltstone (Figure 9A,C), and an intervening phase 2 where the microbial buildup intertongues with detrital intermound facies (Figure 9A). Scaling of vertical relief and siltstone onlap from drone images indicates that synoptic relief evolved from 1.6 to 4 m in phase 1, decreased

to a maximum of 0.5 m in phase 2 and increased again to 3.5–5.4 m in phase 3. The minimum estimates reported here for phases 1 and 2 are based on buildup relief that is directly overlapped by siltstone. Maximum estimates include relief that can be traced on the outer buildup contact above the level of overlapped siltstone. No corrections were made for compaction. Tongues of material shed from microbial phase 2 are mud-poor packstone with angular microbial-micrite clasts, peloids and minor skeletal fragments (Figure 9E). Intermound facies deposited concurrent with phase 2 microbial growth consists of skeletal and oolitic packstone to grainstone with intercalated beds of heterolithic facies (Figures 3 and 9A). Grainstone is massive to cross-bedded, whereas the

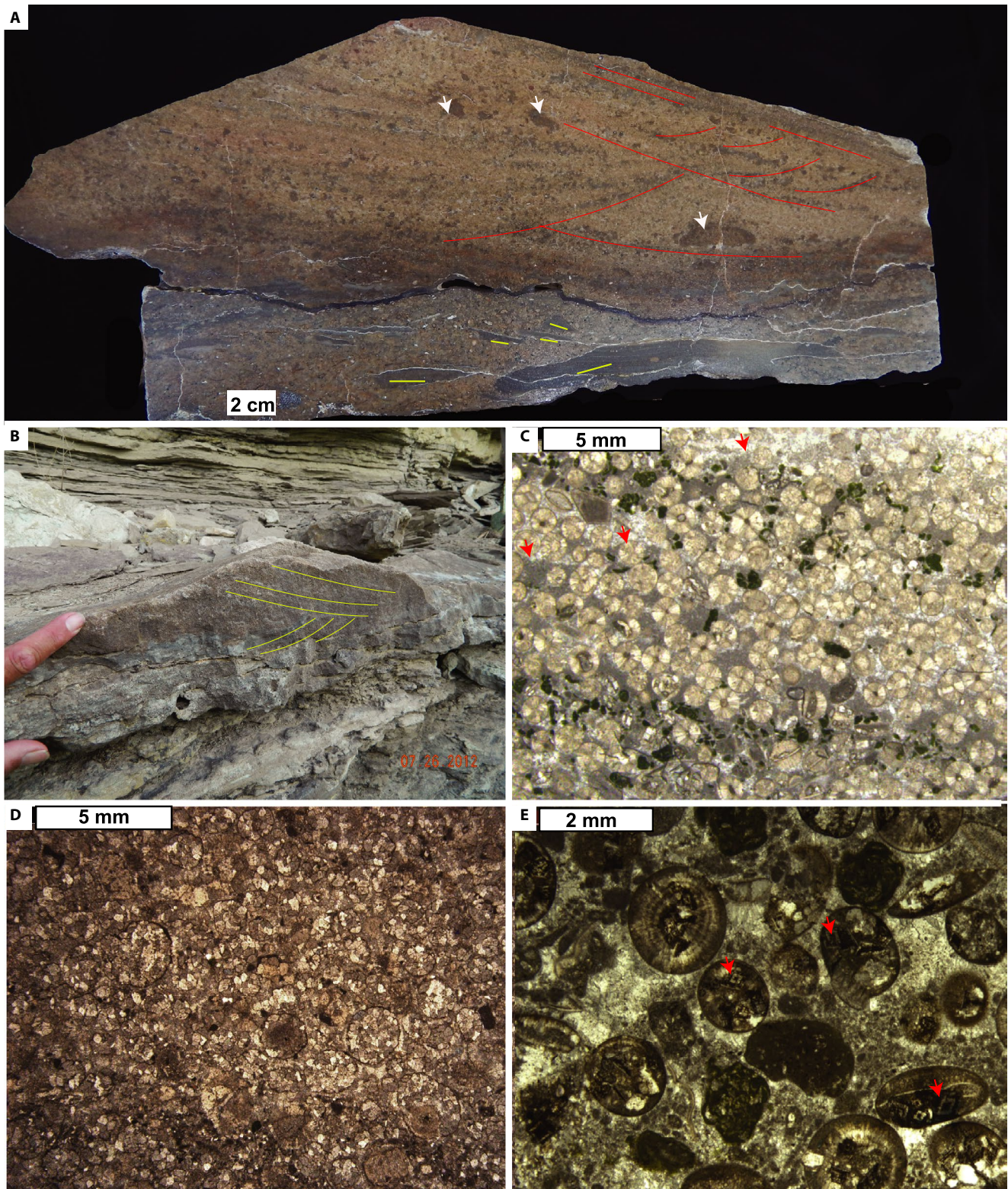


FIGURE 10 Oolitic packstone to grainstone. (A) Polished slab, sample cut perpendicular to ripple crest, from asymmetric megaripple in oolitic grainstone from Mill Creek Section 15.9 m. Cross bedding with erosive reactivation surfaces and reversing current directions (red lines). Pebble-size oolitic grainstone intraclasts (white arrows). Oolitic grainstone overlies flat-pebble conglomerate with imbricated clasts (yellow lines). (B) Outcrop photograph of asymmetric megaripple in oolitic grainstone. Mill Creek Section, 15.9 m. (C) Oolitic skeletal packstone. Carbonate mud infiltrated into intergranular porosity forming geopetal fabrics (arrows). Ooids have radial cortical fabrics. Thin section, cross-polarized light. Bank House Section, 0.89 m. (D) Oolitic skeletal grainstone. Ooids recrystallized and dolomitized. Preserved as ghost fabrics. Thin section, plane-polarized light. Shepard Pavement Section, 0.5 m. (E) Oolitic skeletal packstone. Peloidal sediment between ooids. Ooids have radial cortical fabrics and are micritized at the outer edge. Ooids are partially replaced by dolomite (arrows). Droxrock Flank Section, 2.92 m. Thin-section, cross-polarized light

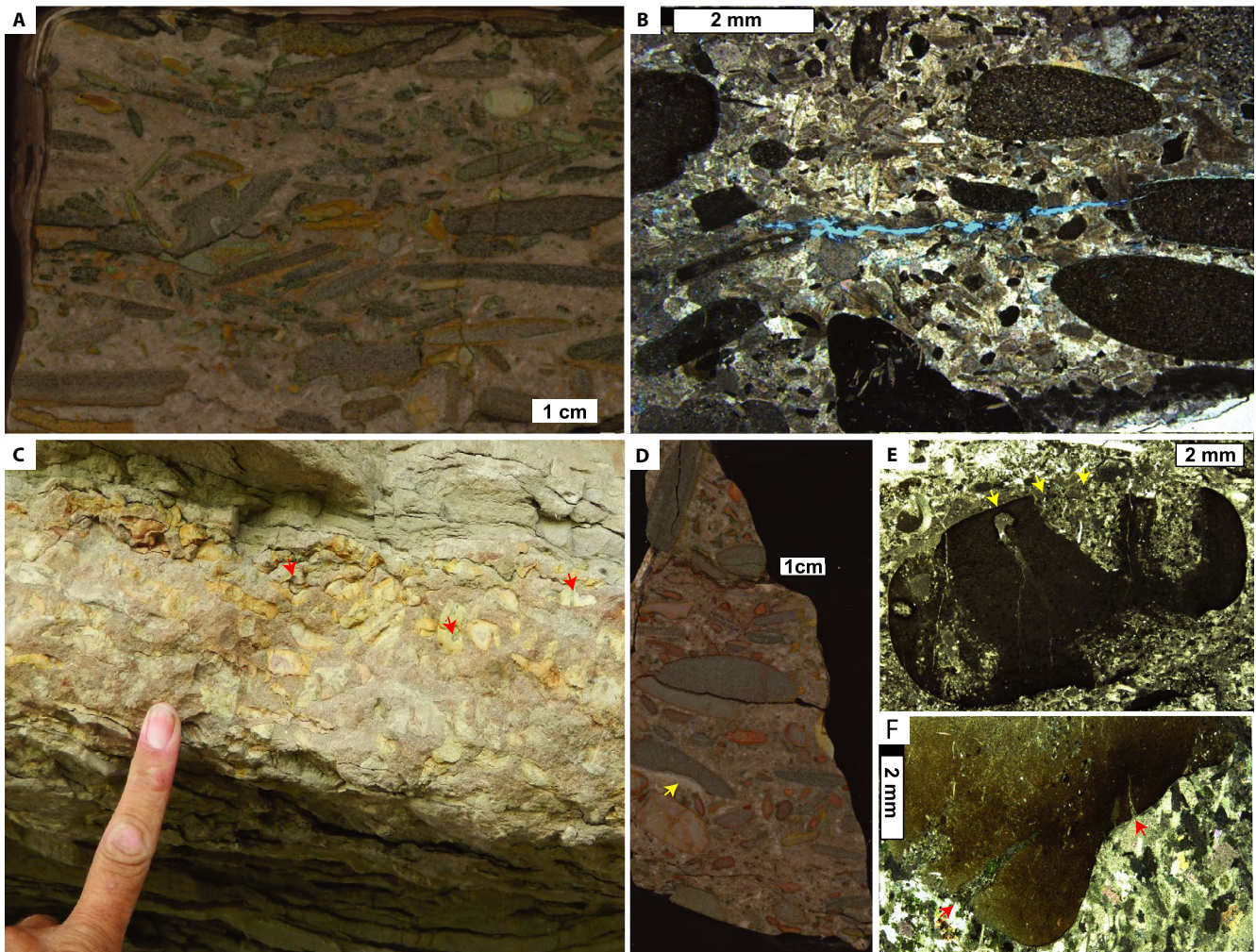


FIGURE 11 Intraclastic conglomerate. (A) Intraclastic conglomerate composed of rounded to subangular flat pebbles composed of laminated heterolithic facies. Subhorizontal orientation and crude imbrication (centre). Polished slab. Fallen Blocks Section, 0.79 m. (B) Intraclastic conglomerate composed of rounded flat pebbles with skeletal grainstone matrix. Thin-section, cross-polarized light. Fallen Blocks Section 3.63 m. (C) Intraclastic conglomerate composed of equant micritized clasts with oxidized and irregular embayed margins. Circular holes and embayments in clasts are interpreted to be borings (arrows). Mill Creek Section, 20.5 m. (D) Intraclastic conglomerate composed of a combination of micritized equant clasts and rounded flat pebbles. Shelter porosity beneath clasts filled with calcite spar (arrow). Polished slab. Fallen blocks Section, 3.63 m. (E) Micritized and oxidized clasts from intraclastic conglomerate. Edge of clast outline (arrows) shows partial micritization of skeletal grainstone clast. Thin-section, cross-polarized light. Mill Creek Section, 20.5 m. (F) V-shaped cracks in the margin of clast (arrows). Cracks show that shrinkage occurred during diagenetic alteration. Thin-section, cross-polarized light. Mill Creek Section, 20.5 m

packstone contains burrows. Skeletal material is bioclastic trilobite, eocrinoid and brachiopod debris.

Decimetre-scale stromatolitic columns are the dominant component in the interiors of the buildups during all three phases of evolution (Figures 9B,D, 13C and 14A). The interior of the stromatolitic columns are partially or fully dolomitized and contain centimetre-scale clots and micritized burrow tubes 5 mm in diameter (Figure 13C,E). In thin section, the fabric contains clots of microbial-micrite and peloidal-micrite masses with fenestral cavities (Figure 14B,C), and micritized burrow tubes with backfilled sediment containing skeletal fragments in the tube (Figure 14D). The stromatolitic columns range in plan view from simple circular structures (Figure 13C) to complexly infolded (invaginated) structures

(Figure 13D). The invagination of these structures is interpreted to be the plan-view expression of branching. In cross section this complexity is represented by vertical columns that diverge and branch and coalesce vertically (Figure 9D).

Thin sections of the stromatolite columns within the interior of the mounds contain traces of entrapped trilobite and eocrinoid fragments but lack a siliciclastic component (Figure 14B). The dense micritic and finely clotted thrombolitic rind enveloping intermediate and large mounds (Figure 9B) is undolomitized (Proctor *et al.*, 2019) and contains the best-preserved microbial microfibrils. Although the rind appears to be leolite in outcrop (Figure 9B,C), polished slabs and thin section show the rind contains finely clotted thrombolite with millimetre-scale clots composed of *Tarthinia* and *Girvanella* (Figure 14E,G).

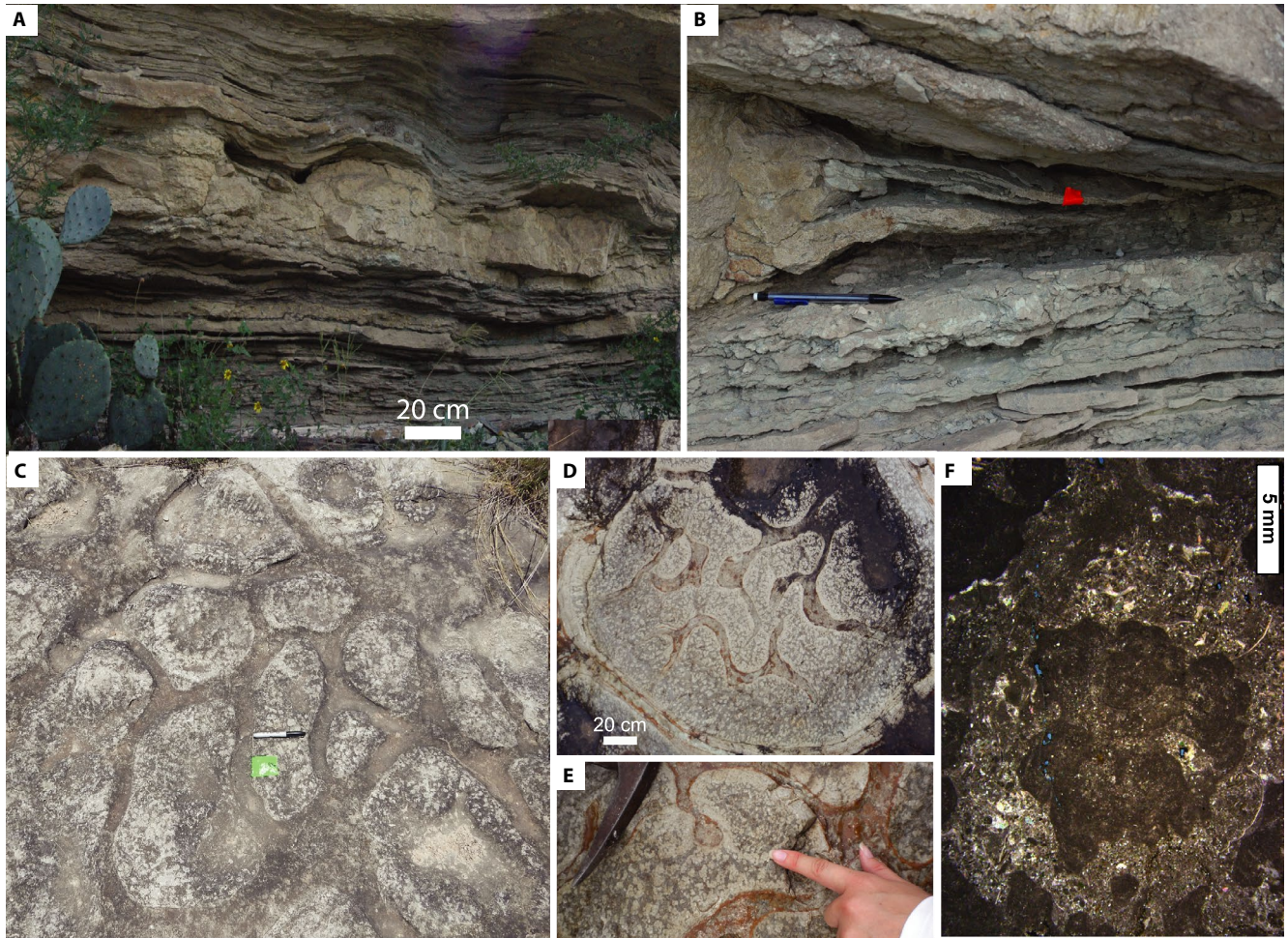


FIGURE 12 Microbial boundstone, small mounds and biostromes of the lower Point Peak Member. (A) Small microbial mounds nucleated on flat-pebble conglomerate and intertongued laterally with heterolithic facies. Mill Creek Section, 17 m. (B) Margin of small microbial mound illustrated in (A). Shown are intraclastic conglomerate substrate of mound, and lateral intertonguing of mound with heterolithic facies. Pen is 14 cm. Mill Creek Section, 17 m. (C) Fitted shapes of thrombolites in biostrome formed by coalesced growth. Shepard Pavement Section, 1.9 m. Pen is 14 cm. (D) Biostrome with complexly invaginated “meandroid” thrombolites. Clots are composed of microbial micrite separated by entrapped gray detrital sediment. Shepard Pavement Section, 7.7 m. (E) Close up of margin of thrombolite shown in (D). Clots merge together to form dense micritic rind at edge of microbial structure. (F) Thin section of micrite microbial clot (centre) and entrapped detrital carbonate and siliciclastic silt. Cross-polarized light. Shepard Pavement Section, 7.7 m

A spectral gamma-ray log through the interior of the Droxrock buildup has very low total gamma ray and thorium values, with a subtle progressive upward increase indicating very low siliciclastic content (Figure 3). Elemental proxy data for siliciclastic flux (e.g. Al, Si, Ti) have low concentrations with no systematic upward increase through Droxrock, and minor increases along stylolites at phase boundaries (e.g. 7% Al_2O_3 at the top of phase 1) indicating a possible increase in siliciclastic clay at the phase boundaries (Swartz *et al.*, 2017).

4.2 | Stratigraphic cyclicity

Stratigraphic cyclicity in the Mill Creek composite section is interpreted from the facies succession in the stratigraphic

log and from spectral gamma ray profiles (Figure 15). Sedimentary structures, texture and biotic composition of facies support the interpretation that siliciclastic and heterolithic facies formed in nearshore environments whereas skeletal, oolitic and microbial carbonate facies formed primarily in offshore marine environments (Table 1). Transgressive–regressive curves were interpreted from the facies associations indicating cyclic shifts between siliciclastic and heterolithic facies representing nearshore regressive stages, and skeletal, oolitic and microbial carbonate representing transgressive stages (Figure 15).

The analysis yields a low-frequency transgressive–regressive cycle with maximum transgression occurring in the carbonate dominant interval in the uppermost Morgan Creek and lower Point Peak members, followed by

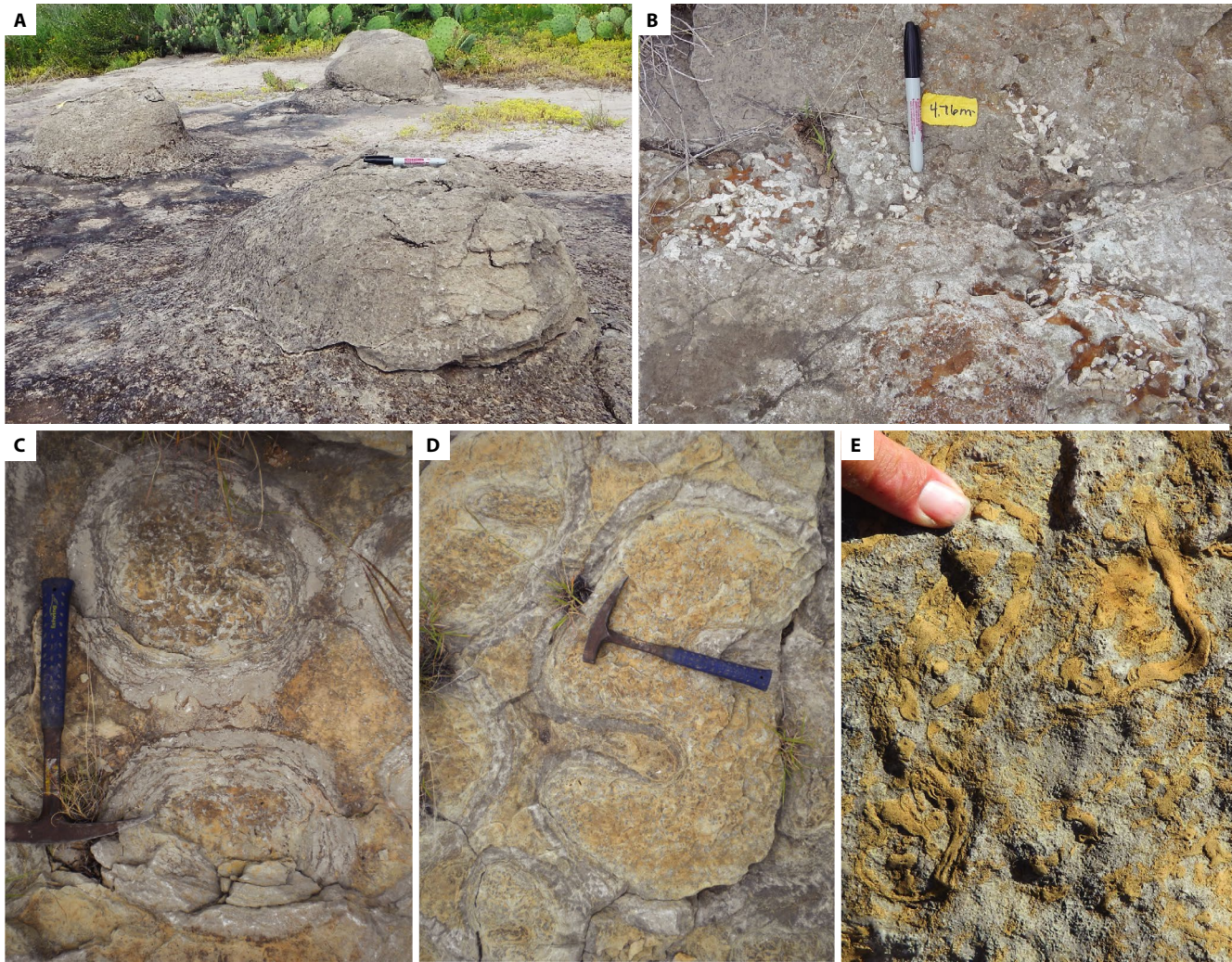


FIGURE 13 Microbial boundstone structures. (A) Small isolated microbial mounds nucleated on a hardground pavement. Mounds have been exhumed by erosion of siltstone that onlapped and buried the mounds. Pen is 14 cm. Shepard Pavement Section, 4.8 m. (B) Eocrinoid holdfasts on submarine hardground that provides substrate for nucleation of microbial mounds. Pen is 14 cm. Shepard Pavement Section, 4.76 m. (C) Stromatolitic columns that occur within the interior of large microbial mounds in the upper Point Peak. Clotted and dolomitized interior region (orange colour) and undolomitized outer stromatolite. Hammer is 33 cm. Zesch Pavement Locality. (D) Stromatolitic columns with complex infolded (invaginated) geometry within the interior of large microbial mounds in the upper Point Peak. Shown are clotted and dolomitized interior (orange colour) and undolomitized outer stromatolite. Hammer is 33 cm. Zesch Pavement Locality. (E) Dolomitized tube structures, interpreted to be burrows within the clotted interior of stromatolitic column in large microbial mound in the upper Point Peak. Droxxrock Locality

regression in the siliciclastic-dominated middle Point Peak, and transgression again in the upper Point Peak (Figure 15). A complete low-frequency cycle in the Point Peak Member is 44 m thick. The Morgan Creek Member contains the upper part of another low-frequency cycle (Figure 15). Intermediate-frequency cycles with an average thickness of 7.4 m were also interpreted from changes in facies from the section and gamma ray profile (Figure 15). The section contains six complete and two partial intermediate-frequency cycles. It was impossible to define high-frequency cycles at the metre scale because there is no consistent fining-upward, coarsening-upward or shallowing-upward facies motif (Figure 15 and Figure S1). Markov chain analysis indicates that the facies transitions are ordered (rule out

null hypothesis of randomness at 95% confidence interval) at the scale of the low-frequency cycles, and for three out of seven of the intermediate cycles (Figure 15). Random facies transitions are indicated at the metre-scale indicating the lack of statistically ordered facies successions at the scale of high-frequency cycles (Figure 15). Markov chain analysis at the scale of low to intermediate-frequency cycles indicate significant associations (transitions) between heterolithic–intraclastic–siliciclastic facies and skeletal–oolitic–microbial facies supporting the interpretation of a cyclic alternation between facies interpreted to represent nearshore vs. offshore environments (Table 1). The fact that some of the qualitatively defined intermediate-frequency cycles and all metre-scale facies successions fail to reject

the null hypothesis of randomness indicates that random processes operated at the higher frequencies (Figure 15).

5 | INTERPRETED DEPOSITIONAL ENVIRONMENTS

5.1 | Siliciclastic facies

Fine to medium sandstone and fine sand to siltstone facies are interpreted to represent marine nearshore tidal-flat environments with an aeolian sourcing of siliciclastic detritus to the shoreline. Siliciclastic facies are dominantly composed of laminated siltstone nearly identical in aspect and are associated with heterolithic facies interpreted to represent intertidal deposition across an expansive tidal flat with low wave-energy. The dominant horizontal lamination and angular silt size quartz, feldspar grains and the presence of mica support low-energy deposition.

Sandstone is subordinate and concentrated within the upper Morgan Creek and middle Point Peak (Figure 3 and Figure S1). Traces of marine skeletal fragments demonstrate marine deposition. Well preserved, but relatively rare wave-oscillation ripples occur associated with heterolithic and carbonate facies within the lower Point Peak (Figures 3 and 4E and Figure S1) unambiguously demonstrating wave agitation in a very shallow-water shoreline environment. Rare, thin intervals of glauconitic siltstone are extensively burrowed indicating the presence of a low-energy subtidal environment probably just seaward of the tidal flat. Concentration of medium to fine sand within the upper Morgan Creek may reflect long-term trends in sea-level fluctuation. Sand occurrence generally diminishes upward in the Morgan Creek to Point Peak reflecting transgression of the Sauk III supersequence (Figure 1B, Morgan, 2012).

The aeolian delivery of siliciclastics to the depositional system is supported by the narrow range of grain size, the paucity of a clay fraction and by analogy to an aeolian interpretation for the deposition of the older Hickory Sandstone in the Llano area (McBride *et al.*, 2002; Kyle and McBride, 2012). Aeolian delivery of siliciclastics to marine nearshore environments has been interpreted in several other studies of the GACB (Dott *et al.*, 1986; Chow and James, 1987a; Myrow *et al.*, 2004; Runkel *et al.*, 2007, 2012) and should be important as there were expansive, non-vegetated upland areas such as the transcontinental arch and various cratonic arches capable of providing an aeolian supply of sediment to epeiric seas.

5.2 | Heterolithic flaser-bedded siltstone–packstone

Heterolithic siltstone to packstone is interpreted to represent generally low-energy intertidal deposition across an expansive

tidal flat. Flaser bedding consisting of intercalations of horizontally laminated siltstone and lenticular to continuous carbonate packstone layers is interpreted to represent repeated flooding and emergence by tides. Silt drapes are interpreted to represent slack tide. Carbonate packstone beds contain pebbles, skeletal debris and glauconite reflecting marine influence. Reversing current indicators in ripple cross-laminated lenses reflect flood and ebb tidal currents. Carbonate beds containing thinning and thickening-upward coarse-fine lamination are interpreted to represent spring-neap tidal bundles (Tape *et al.*, 2003). Desiccation cracks indicate emergence of the tidal flats during low tide. Similar flaser-bedded heterolithic facies have frequently been interpreted to be an intertidal component of the Cambro-Ordovician peritidal cycles (Goldhammer *et al.*, 1993; Demicco and Hardie, 1995) and tidal influences have been widely recognized within the interior of the GACB (Tape *et al.*, 2003; Runkel *et al.*, 2012).

Desiccation cracks are relatively rare within the heterolithic facies and were commonly seen only in cross section. The desiccation cracks are preferentially preserved in carbonate interbeds within the heterolithic facies (e.g. Figure 6C,E). The paucity of clay in the system may have prohibited the formation and preservation of desiccation cracks within the siltstone component of the heterolithic facies; carbonate mud content and early lithification of carbonate interbeds enabled the formation and preservation of desiccation cracks. Although desiccation cracks had not been previously reported, Ahr (1967) and Spincer (1997) interpreted the heterolithic facies as intertidal, and Ahr (1967) interpreted associated flat-pebble conglomerates to be composed of clasts reworked from desiccation polygons from tidal flats. Abundant rounded clasts of heterolithic facies within the associated intraclastic conglomerate facies demonstrate early lithification, especially of carbonate-rich layers on the tidal flat. Reworking of clasts into intraclastic layers is interpreted to have occurred during storms.

Mud cracks in the Mesoproterozoic Belt Supergroup with a variety of polygonal, linear and spindle-shaped geometries, previously assumed to be desiccation structures, have been reinterpreted to be seismite deformation structures in which the cracks formed as fluidized sand was injected upward and downward into intercalated mud layers (Pratt and Ponce, 2019). The cracks reported herein from the Mill Creek and Fallen Blocks sections, however, are V-shaped structures that penetrate downward from the tops of beds and are filled with sediment from above consistent with an origin as desiccation features (Figure 9). Furthermore, the sandstone–siltstone and heterolithic facies contain a suite of structures indicative of very shallow water and peritidal environments (small symmetrical ripples, flaser bedding with reversing current indicators, silt drapes and tidal bundling) consistent with the interpretation that cracks in the Point Peak Member formed by desiccation.

5.3 | Skeletal packstone to grainstone

Skeletal packstone to grainstone is interpreted to represent open-marine subtidal environments based on a stenohaline biota of trilobites, eocrinoids and brachiopods. High-energy currents are reflected by a grainy texture and the common occurrence of cross-bedding and megaripples. Skeletal grains in packstone and grainstone are entirely fragmental and often broken and rounded (Figure 7), and commonly contain adhered carbonate mud indicating that they were initially deposited in a lower energy environment and reworked by currents or wave action. Brachiopods are less abundant compared to trilobite and eocrinoid fragments in the skeletal packstone–grainstone (Table 2) and commonly are found disarticulated in local concentrations on bedding planes and troughs between megaripples indicating they may represent local living assemblages or were hydrodynamically concentrated.

Skeletal grainstone is interpreted to have been deposited in offshore subtidal shoals and sheets influenced by tidal currents forming megaripples and cross bedding with reversing current indicators (Figures 5 and 7). Storms are interpreted to have reworked the skeletal detritus into thin laterally extensive sheets across the shelf. Background deposition following storm events allowed carbonate mud to infiltrate the intergranular porosity and for bioturbation to mix in carbonate mud forming packstone. Lenses of dolomitized micrite represent lower energy conditions following storms and during slack tide. Presumably, trilobites and eocrinoids lived and were originally deposited in a low-energy environment further offshore prior to being reworked by high-energy currents and waves. Skeletal material is fragmented, broken and rounded. Either the sections measured in the study area formed entirely shelfward of such a low-energy environment or the sections represent amalgamated storm deposits resulting from repeated storm recycling of sediments and obliteration of low-energy background sedimentation. Bioclastic sands composed of trilobite, eocrinoid and brachiopod debris are common in Cambrian epicratonic sequences and have been commonly interpreted to reflect transport and deposition by storms and other high-energy currents (Palmer, 1989; Myrow *et al.*, 2004; Pratt and Bordonaro, 2007; Labaj and Pratt, 2016; Runkel *et al.*, 2012).

5.4 | Oolitic packstone to grainstone

Oolitic packstone to grainstone is interpreted to represent open-marine subtidal, tide-agitated shoals reworked into sheet deposits by storms similar to the skeletal packstone–grainstone facies (Figure 3, Table 1). Megaripples with reversing current indicators provide clear evidence for tidal-current agitation (Figure 10). Megarippled beds are grainstone and

contain oolite lithoclasts indicating active tidal agitation of shoals, marine lithification and reworking of clasts, similar to modern analogues (Harris, 2019). Ooids likely formed in high-energy, tide-agitated shoals in an offshore subtidal setting (Khanna *et al.*, 2019). The very thick bed of oolitic skeletal grainstone formed coeval with the base of the large microbial mounds in the upper Point Peak (Figures 3, 8A and 9A) is interpreted to represent such offshore shoals with associated microbial mounds.

Thin oolite beds (0.16–0.46 cm thick) within the Morgan Creek, lower Point Peak and upper Point Peak (Figure 3) are interpreted to record sediment reworking by storms into sheet deposits across the shelf. After storm reworking, tidal currents resumed forming the megaripples that commonly cap the thin layers. Lower energy conditions in troughs of megaripples, or during pauses in currents allowed the accumulation of lenses of carbonate mud. Thin ooid packstone beds with micritized ooids, admixed skeletal fragments, peloids and carbonate mud infiltrated into intergranular porosity are interpreted to represent the waning energy following storms. Similar aprons of ooid packstone with admixed peloids and carbonate mud have been interpreted from modern analogues to represent oolitic deposits washed into the platform interior from the high-energy shoal environment of active ooid genesis (Harris, 2019). Orientation plots of the crests of megaripples compiled from skeletal and oolitic grainstone beds from the lower and upper Point Peak Member show a relatively wide spread in palaeocurrent directions with a dominant NE–SW trend (Figure 3).

Ooids in the Point Peak Member have nuclei composed of peloids or skeletal fragments and lack quartz nuclei supporting the interpretation that the offshore zone of ooid formation may have been beyond the reach of siliciclastic sand flux. Ooids have well preserved radial cortices indicating Mg-calcite mineralogy (Chow and James, 1987b).

5.5 | Intraclastic conglomerate

Intraclastic conglomerate beds within Morgan Creek and Point Peak are interpreted to have several origins. The most common conglomerate beds are sheets and broad, flat channelized deposits composed of rounded, tabular (flat pebble) clasts of heterolithic facies and equant, irregular, embayed and oxidized clasts (Figure 11). The broad, low-relief channels (up to 30 cm deep and several metres across) are cut into heterolithic facies and are interpreted to represent erosion and channelization during storm-surge onto tidal flats. The low relief of the channels and absence of features indicating lateral migration is incompatible with tidal channel origins (Shinn, 1983, 1986). Imbrication of clasts, and shelter porosity beneath tabular clasts are consistent with deposition by traction currents during storms.

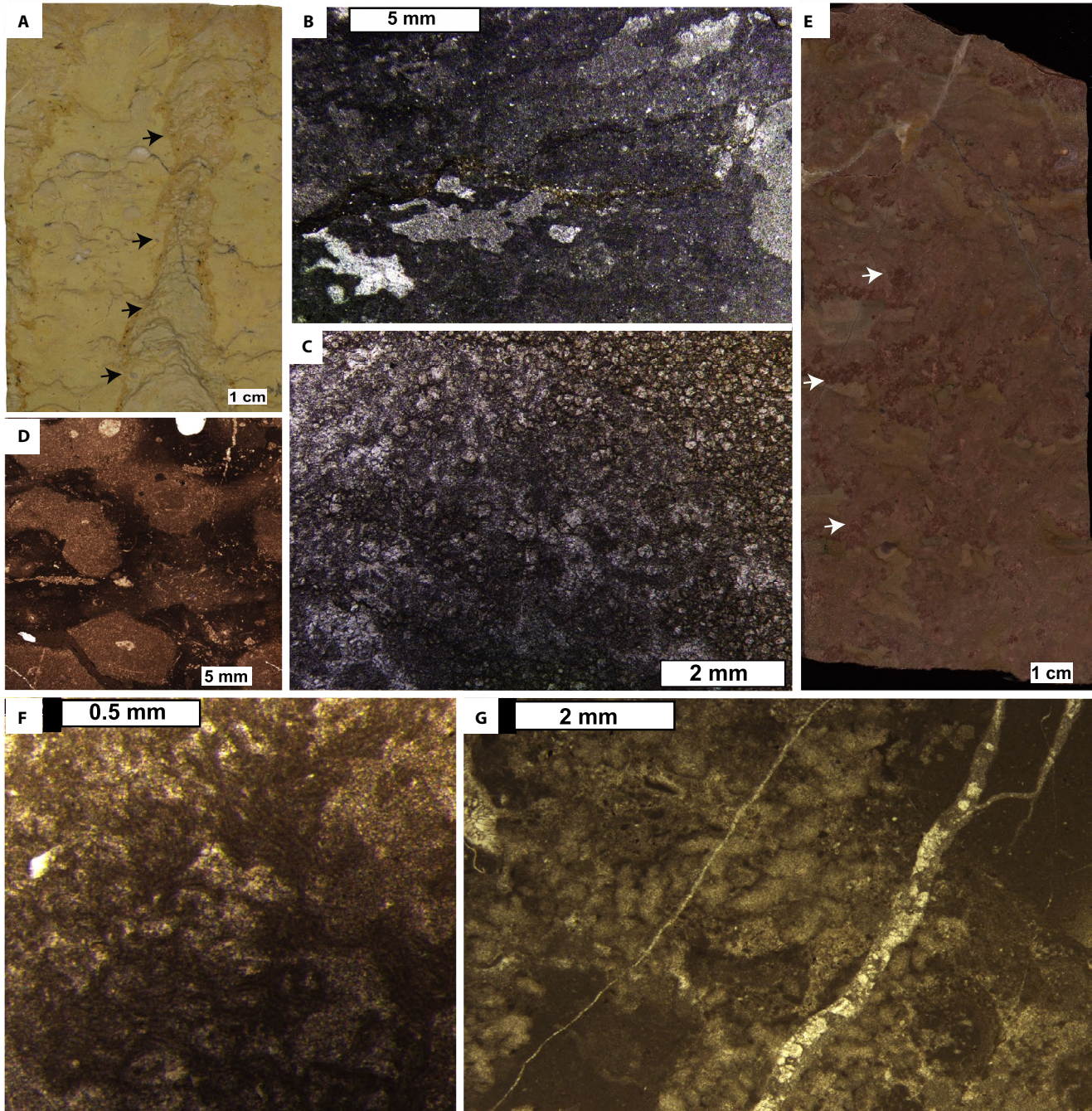


FIGURE 14 Microbialite fabrics in the large mound interval of the upper Point Peak Member at Droxford. (A) Stromatolitic column (arrows) surrounded by irregularly clotted thrombolite. Polished slab, phase 2. (B) Thrombolite fabric illustrating dense micritic and peloidal microbial clots and fenestral cavities. Thin-section, plane polarized light. Phase 2. (C) Thrombolite fabric illustrating partially dolomitized peloidal microbial clots. Thin-section, plane polarized light. Phase 2. (D) Burrow tubes in thrombolite. Tubes are preferentially dolomitized micrite containing skeletal fragments (interpreted to be backfills). Burrows typically have a central tube filled with spar. Thin-section, cross-polarized light. (E) Calcimicrobial framework (arrows) within dense micrite of the rind surrounding phase 1 of the large microbial mound at Droxford. Polished slab. (F) Calcimicrobial framework fossil *Girvanella* in the dense micrite of the rind surrounding phase 1 of the large microbial mound at Droxford. Thin-section, plane polarized light. (G) Calcimicrobial framework fossil *Tarthinia* in the dense micrite of the rind surrounding phase 1 of the large microbial mound at Droxford. Thin-section, plane polarized light

The intraclastic conglomerates are intercalated with heterolithic facies (Figure 3 and Figure S1). The rounded flat pebbles are interpreted to represent erosion and reworking of partially lithified clasts from the heterolithic facies. The

equant micritized clasts are interpreted to have been reworked from subtidal hardgrounds. The equant aspect reflects origin from a more homogeneous, non-tabular skeletal facies rather than the heterolithic facies. Micritization and oxidation of

Mill Creek composite section

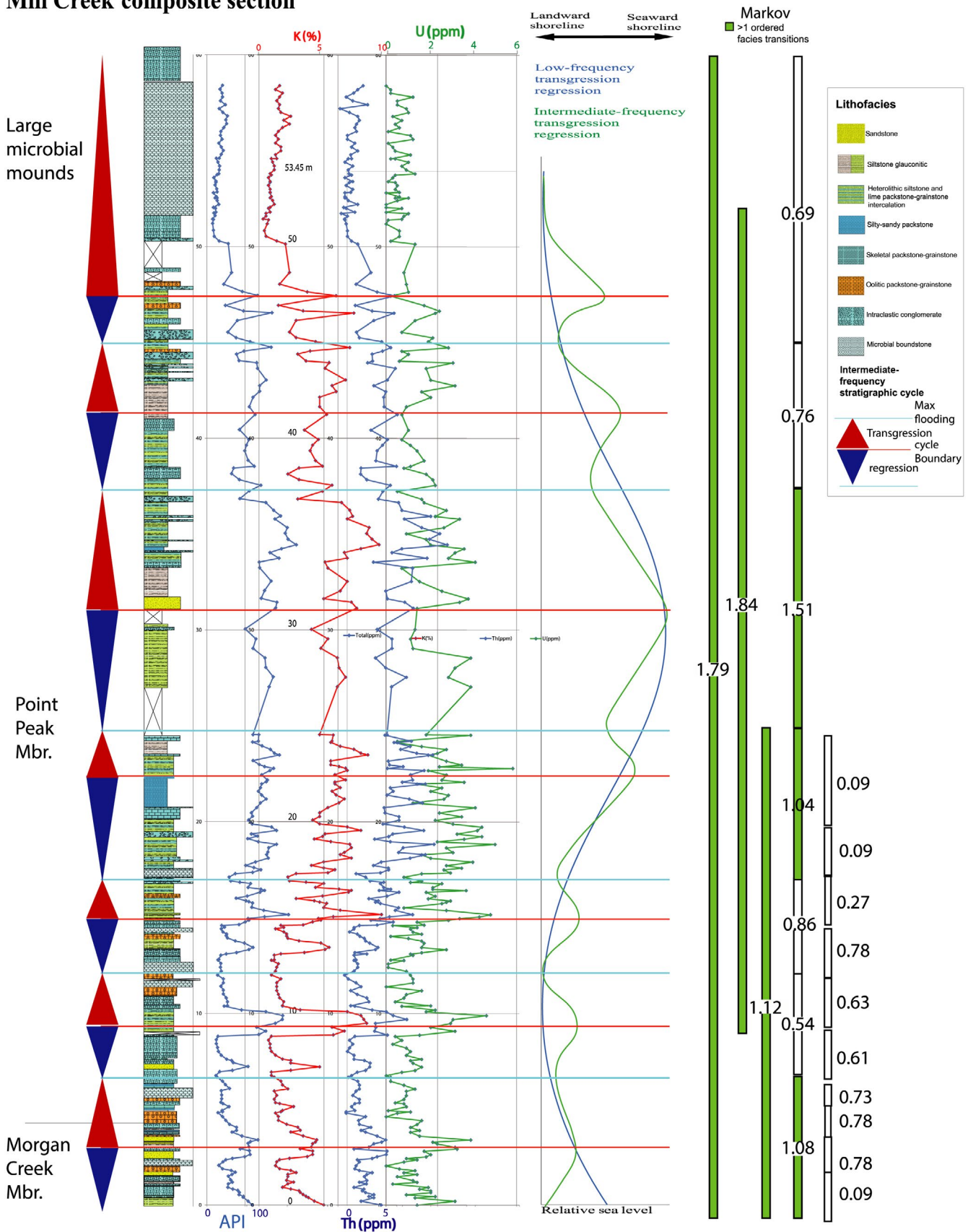


FIGURE 15 Mill Creek Composite stratigraphic section with spectral gamma ray logs and interpretation of stratigraphic cycles. Integrates stratigraphic data from individual sections of Figure 3 into a composite section. Transgressive–regressive curve interpreted from facies associations and depositional environments (Table 1). Statistics from Markov chain analysis shown at right. Green bars indicate ordered facies transitions. Numerical values are chi-squared statistic normalized to chi-squared statistic that must be exceeded to rule out null hypothesis of randomness at 95% confidence interval. Values greater than 1 indicate ordered vertical facies transitions at 95% confidence interval

some clasts is only partial, suggesting that the original lithology was skeletal packstone–grainstone (Figure 11E). Regular rounded embayments in clast margins are interpreted to represent borings. Pitted, micritized, irregularly embayed and oxidized margins of the micritic clasts reflects hiatus, long residence time and diagenetic alteration of the clasts (Figure 11). The clasts are interpreted to have been reworked from micritized, mineralized (possible glauconitization that was later oxidized) and bored hardgrounds.

Localized occurrences in the upper Point Peak Member of edge-wise “pin wheel” flat-pebble conglomerates with highly organized, radially distributed imbrication are interpreted to have been deposited by complex eddies in traction currents (Ahr, 1967) or by wave action in beach deposits by analogy to similar modern deposits (Demicco and Hardie, 1995). Finally, the flat-pebble conglomerate unit at the base of the very thick, skeletal oolitic grainstone bed and at the base of the large microbial mounds is interpreted to represent a transgressive lag-deposit composed of clasts eroded from the base of the underlying heterolithic facies (Figures 3, 8A and 9A; Khanna *et al.*, 2019). The stratigraphic position at the base of a widespread transgressive ravinement surface and a major shift in the depositional system supports this interpretation (Figure 15).

A wide variety of mechanisms have been proposed for the genesis of flat-pebble conglomerates (Demicco and Hardie, 1995; Myrow *et al.*, 2004; Alvaro and Clausen, 2007; Pratt and Bordonaro, 2007). Mechanisms incompatible with field observations made during this study include slumping and gravity flow of partially lithified beds (Myrow *et al.*, 2004), lags within migrating tidal channels (Demicco and Hardie, 1995) and transgressive lags at the base of high-frequency metre-scale cycles (Demicco and Hardie, 1995). Deposition as tsunamites (Pratt and Bordonaro, 2007) is a model compatible with field observations. However, because of the tectonically stable palaeogeographic setting and the lack of any stratigraphically unusual context that would support tsunami deposition, this mechanism is considered unlikely here.

5.6 | Microbial boundstone

Microbial boundstone is interpreted to form both in nearshore marine intertidal and shallow-subtidal environments forming thin intervals of mounds and biostromes associated with heterolithic facies in the lower Point Peak, and as larger offshore, open-marine subtidal mounds represented in the upper Point Peak (Figure 15).

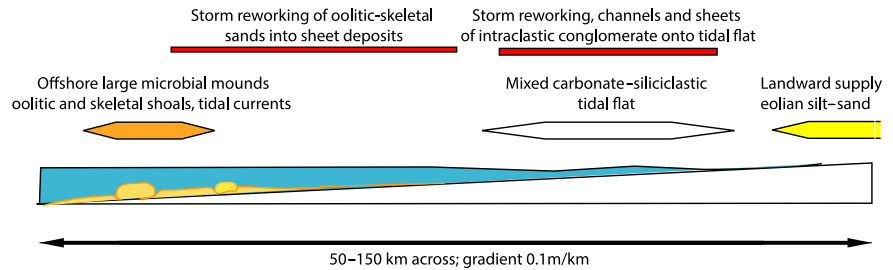
Small microbial mounds in the lower Point Peak Member exposed along the Mill Creek cliff interfinger with heterolithic facies demonstrating that they formed in a marine tidal-flat environment concurrent with heterolithic deposition (Figures 5 and 14). Detrital sediment deposited in the

passages between small mounds and within biostromes in the Shepard Pavement section contains alternations of skeletal–oolitic grainstone, siliciclastic silt and carbonate mud, indicating fluctuation in current energy. These are interpreted to be oscillations between high and low current energy consistent with flood-ebb and slack tide conditions on a tidal flat. Siliciclastic silt associated with the microbial structures is consistent with siliciclastic flux into the nearshore intertidal environment. Individual mounds coalesce laterally along the Mill Creek cliff outcrop to form laterally continuous biostromes (Figure 5). The lateral coalescence into thin biostromes is interpreted to reflect low accommodation-space in the nearshore setting. The isolated mounds in the lower Point Peak at the Shepard Pavement section are nucleated on a skeletal grainstone hardground surface (Figure 13) and have up to 0.9 m of synoptic relief overlapped by siliciclastic siltstone (Figures 3 and 13). These are interpreted to have been deposited in subtidal environments seaward of the tidal flats.

Microbial mounds in the upper Point Peak Member are interpreted to have formed further offshore in an open-marine environment with greater accommodation. Greater accommodation is supported by greater thickness, up to 7.7 m at Droxrock and up to 14 m at James River (Khanna *et al.*, 2019), as well as greater synoptic relief (up to 5.4 m; Figures 3, 9 and 15). The presence of a stenohaline fauna consisting of trilobite and eocrinoid fragments trapped within the mound and in associated oolitic–skeletal grainstones supports an open-marine interpretation. The low siliciclastic detrital component in the mounds can be explained by an offshore position. Khanna *et al.* (2019) interpreted a 10–15 m water depth in the environs of the large mounds based on an analysis of the amplitude of subaqueous dune forms in associated carbonate grainstone.

The interpreted three-phase evolution of the large microbial buildups, supported by margin architecture (Khanna *et al.*, 2019), indicates that the buildups developed greater synoptic relief and sharp-walled margins with a dense micritic and finely clotted thrombolitic rind in phases 1 and 3, separated by an interval of lesser synoptic relief and intertonguing with intermound detrital sediment during phase 2 (Figure 9). Phase 1 is interpreted to have occurred concurrent with oolitic skeletal grainstone deposition represented by the very thick grainstone bed adjacent to and underlying the microbial buildups (Figures 3, 8A and 9A; Khanna *et al.*, 2019). Upward growth of the buildups resulted in increasing synoptic relief above intermound detrital carbonate sediment and a sharp-walled geometry (Figure 9A). A pause in carbonate deposition and influx of siliciclastic silt overlapped the sharp margin prior to phase 2 growth that occurred with lesser synoptic relief and concurrent with the accumulation of intermound detrital carbonate and siliciclastic sediment (Figures 3 and 9A; Khanna *et al.*, 2019). This was followed by a sharp walled phase 3 nearly identical to phase 1 (Figure 9).

FIGURE 16 Simplified depositional model summarizing interpretation of depositional environments and influence of tides and storms



6 | DISCUSSION

6.1 | Depositional model

From detailed interpretations of depositional environments, facies associations and stratigraphic succession (Figure 15), in the context of deposition on the GACB, the Morgan Creek and Point Peak members are interpreted to have been deposited on a broad, low-angle, mixed carbonate–siliciclastic ramp system (Figure 16). The inner ramp was dominated by aeolian deposition of siliciclastic sand and silt and tidal-flat environments with siliciclastic–carbonate heterolithic facies gradually changing seaward to low-relief microbial mounds and biostromes. The middle ramp portion was dominated by subtidal shelf deposition with small isolated microbial mounds and sheets of skeletal–oolitic sand. Deposition in the offshore zone consisted of skeletal and oolitic sand shoals and large microbial mounds formed in open-marine environments with vigorous tidal currents and storm agitation (Figure 16). Most of the biotic component, dominated by trilobite and eocrinoids, lived in and was initially deposited in low energy environments, possibly further offshore in deeper-water environments prior to being reworked as skeletal debris.

Using a regional slope gradient of 0.1 m/km for the epicratonic ramp of the GACB (Runkel *et al.*, 2007, 2012), the distance across the ramp from the intertidal zone to the zone of subtidal shoals and large microbial mound development is interpreted to have been *ca* 50–150 km based on minimum and maximum water depths estimated for large mound deposition (Khanna *et al.*, 2019). Relatively high rates of siliciclastic sediment flux into the inner ramp coupled with vigorous reworking of sediment across the shelf by storms and tidal currents are interpreted to have maintained a graded low-angle ramp profile.

The depositional system experienced a dominant tidal influence both on the tidal flat (as evidenced by fluctuating current energy, ripples with reversing current indicators, tidal bundles), and as vigorous agitation of offshore shoals (as evidenced by abundant megaripples with reversing current indicators), as well as extensive wave influence during storm events, as evidenced by reworked sand sheets across the shelf, and broad channel fills of intraclastic conglomerates on the tidal flats. The result is a hybrid tide-dominated

depositional system heavily influenced by storms and also a mixed carbonate–siliciclastic system developed on an extremely low-gradient epicratonic shelf that does not easily classify into end-member depositional models (Dalrymple, 2010; Plint, 2010; Pratt, 2010). Evidence of both tidal and wave influence is well documented from Cambrian epicratonic strata despite debate on the extent of wave and tidal currents in vast epicratonic seas (Klein and Ryer, 1978; Driese *et al.*, 1981; Byers and Dott, 1995; Tape *et al.*, 2003; Allison and Wells, 2006; Eoff, 2014; MacNaughton *et al.*, 2019).

Reworked and rounded skeletal debris, ooids and intraclasts all provide evidence of frequent high-energy recycling. Notably, the skeletal packstone–grainstone contains the greatest proportion of glauconite (Table 2). Glauconite occurs as pellets and glauconitized clasts that also may provide evidence of extensive reworking. The glauconite likely mineralized at or just below the seafloor and was reworked as clasts in the skeletal sands (Chafetz and Reid, 2000; Chafetz, 2007). The presence of reworked oxidized clasts (interpreted to have originally been glauconitized) in intraclastic conglomerates also suggests the occurrence of high-energy subtidal hiatuses and long residence times for reworked clasts (Alvaro and Clausen, 2007; Eoff, 2014).

6.2 | Mixed carbonate–siliciclastic depositional system

Upper Morgan Creek and Point Peak deposition represents a true mixed carbonate–siliciclastic system in which siliciclastic silt and sand were delivered by aeolian deposition on the landward part of the depositional system and mixed with carbonate sediments on the tidal flat and shelf immediately seaward of the tidal flat. All but the oolitic facies contain some siliciclastic silt and sand component (Table 2). The heterolithic facies contains a nearly equal mix of siliciclastic detrital components (Table 2). Small microbial mounds and biostromes contain siliciclastic grains entrapped in the microbial structures, as well as a mix of siliciclastic and carbonate detritus in the passages between the microbial structures. In the total volumetric breakdown from the Mill Creek composite section (Table 3) siliciclastic and carbonate depositional components are subequal with a slightly larger carbonate fraction (46%) and lesser siliciclastic fraction (35%).

The Persian Gulf is the closest modern analogue as a mixed carbonate–siliciclastic, epicontinental tidal flat with silt delivered by aeolian processes (Riegl *et al.*, 2010). In contrast to the Persian Gulf, however, there is no evidence for arid conditions in the Morgan Creek and Point Peak depositional system. A lack of land plants, rather than aridity, likely promoted aeolian delivery of silt to the Cambrian tidal flats. Bradley *et al.* (2018) point out that modern depositional models are inadequate for interpreting pre-vegetation tidal flat systems.

Fluctuation of siliciclastic input is interpreted to have been modulated by transgressive–regressive shifts in the shoreline driven by sea-level fluctuation with greater input of siliciclastic material during the regressive stage (Figure 15, see discussion on stratigraphic cyclicity below). Alternatively, fluctuations in climate, potentially coupled with sea-level fluctuation, may have driven patterns of siliciclastic input to the shoreline. Although the transgressive–regressive model (Figure 15) includes a concept of reciprocal sedimentation (Van Siclen, 1958; Wilson, 1967), carbonate and siliciclastic sediment coexisted and mixed in the tidal flat and shelf, changing only in relative proportion rather than alternating in time as in the traditional model of reciprocal sedimentation (Figures 15 and 16). Similar mixed depositional systems with a landward-dominant siliciclastic component have been described from ancient and modern analogues (Zeccin and Catuneanu, 2017). Spatially mixed systems should be especially common on broad ramps influenced by low-amplitude sea-level fluctuations during green-house climate periods, as such systems would lack the abrupt shutting on and off of carbonate factories from high-amplitude sea-level fluctuation typically invoked in the cyclic reciprocal model.

6.3 | Controls on microbialite genesis

The Morgan Creek and Point Peak members contain microbialite mounds and biostromes formed in both proximal intertidal environments and in offshore subtidal environments. A comparative analysis of these microbialites in the context of their depositional environment and associated sediments, as well as a comparison with modern and ancient analogues, illuminates environmental controls on their genesis.

Stromatolites and thrombolites require a stable, lithified or firm substrate to establish and maintain microbial growth. The Ginsburg and Planavsky's (2008) survey of modern microbialites in the Bahamas revealed a variety of “renewable” substrates formed during deposition such as hardgrounds, firmgrounds and skeletal or cemented clasts. Cambro–Ordovician examples in the Conococheague and Arbuckle groups and Bison Creek and Mistaya formations show that lithified clasts and flat-pebble conglomerates commonly form the substrate for growth of stromatolite and thrombolite mounds (Demicco, 1985; Westrop, 1989; Wilson *et al.*, 1991; Fritz *et al.*, 2012).

Substrates for microbialites in the Point Peak Member include subtidal hardgrounds, flat-pebble conglomerates and skeletal–oolitic packstone to grainstone beds. It is possible that microbialites underlain by skeletal–oolitic packstone to grainstone beds nucleated on undetected hardground surfaces.

It is notable that although there is an association of microbialites formed on flat-pebble conglomerate layers in the Point Peak, there are also numerous conglomerate layers that lack microbial development (Figure 3). This pattern is especially evident in the upper part of the Point Peak Member, below the level of the large microbial-mound development, which contains numerous flat-pebble conglomerate layers intercalated in heterolithic facies (Figures 3, 8 and 9). Obviously, having an adequate substrate does not foster microbial development unless environmental conditions conducive to microbial growth persist after development of the substrate. In this interval, numerous intraclastic conglomerate layers were buried by heterolithic facies in the tidal-flat before environmental conditions could establish microbial growth. Higher in the section, microbial mounds were instead developed on a flat-pebble conglomerate substrate at the base of the very thick bed of skeletal–oolitic grainstone interpreted to be a transgressive lag deposit that also brought a shift to offshore environments conducive to microbial mound genesis (Figure 15, Khanna *et al.*, 2019).

Comparison of intertidal biostromes and small mounds of the lower Point Peak with the large mounds of the upper Point Peak indicates that siliciclastic flux played a relatively minor role in the growth of microbialites. Biostromes and small mounds in the lower Point Peak contain siliciclastic silt trapped within the microbialites and in passageways between mounds (Figure 12). There is no evidence that the siliciclastic flux significantly inhibited growth. Low accommodation space was likely the primary factor that limited vertical growth and encouraged lateral coalescence of mounds into biostromes. The large microbial mounds in the upper Point Peak have a very low siliciclastic content as evidenced by the spectral gamma ray and concentrations of elemental proxies for siliciclastic flux (Figure 3, Swartz *et al.*, 2017). Low siliciclastic content is interpreted to have resulted from their offshore deposition. Development of the three-phase architecture of the large mounds was interpreted by Khanna *et al.* (2019) to have resulted from pulses of siliciclastic sediment flux driven by falls in relative sea level. Proctor *et al.* (2019) reported up to 8% clay content in the large microbial mounds of the upper Point Peak and Swartz *et al.* (2017) reported elemental proxies for greater clay content in stylolites at phase boundaries consistent with such an interpretation. The model of sea-level fluctuation controlling siliciclastic flux and the three-phase architecture of the large mounds (Khanna *et al.*, 2019) also interprets lowering of sea level at the end of each growth phase. No petrographic or geochemical evidence for subaerial exposure at the phase boundaries was found at

Droxrock, indicating that sea-level fall was not great enough to cause emergence of the mounds (Swartz *et al.*, 2017).

Decimetre-scale thrombolitic or stromatolitic mounds and columns are the fundamental elements making up the biostromes and larger microbial mounds (Figures 5, 9 and 13). These features typically form simple columns with circular shape in plan-view but may take on more complexly invaginated shapes (Figures 12 and 13). The invagination seen in plan-view is interpreted to represent vertical branching during growth. Branching and complex-shaped columns have been interpreted to represent lower synoptic relief and sediment infill between columns allowing horizontal growth of columns forming branches, bridges and complex shapes (Bosak *et al.*, 2013). Similar complex maze-like thrombolite structures have been reported from North America and China and have been associated with low synoptic relief (Shapiro and Awramik, 2006; Lee *et al.*, 2014). The complexly invaginated structure is considered to be similar to the maze-like structure although the scale is different with the features in the Point Peak Member being several centimetres to decimetres across rather than centimetres in scale (Shapiro and Awramik, 2006; Lee *et al.*, 2014).

In addition to accommodation space, the rate of intermound detrital infill vs. upward growth of microbial structures affects synoptic relief. The contrast between the sharp-walled mounds that are onlapped by sediment in the small isolated mounds (Figure 13A) or phases 1 and 3 of the large mounds (Figure 9) versus intertongued margins of small mounds (Figure 12) and the intertongued phase 2 of the large mounds (Figure 9A) reflects different rates of intermound detrital sedimentation. Development of sharp-walled mounds indicates a hiatus developed at the margin due to either high-energy bypassing of detrital sediment in the intermound areas or lack of detrital sediment flux as vertical mound growth developed synoptic relief. The sharp-walled rind of phase 1 development of the large mounds, which grew synchronously with oolitic and skeletal sand intermound deposition (Figure 9), resembles deposition of modern large subtidal mounds in the Bahamas, which are repeatedly covered and uncovered by oolitic sediment (Dill *et al.*, 1986). The generally low content of coarse skeletal and oolitic detrital material trapped within the large microbial mounds in the upper Point Peak Member, however, records a striking dissimilarity between the two models.

Individual decimetre-scale mounds within biostromes and stromatolitic columns in the larger buildups contain a dolomitized clotted interior surrounded by a dense, laminar stromatolitic or micritic rind (Figures 9, 12 and 13; Khanna *et al.*, 2019; Proctor *et al.*, 2019). At the decimetre-scale the rind is formed of merged clots of microbial micrite or is stromatolitic (Figure 13). In the intermediate to large-scale mounds the rind is a dense micritic, finely clotted thrombolitic structure containing calcified microbial frameworks of *Tarthinia* and *Girvanella* (Figures 9 and 14).

The contrast between the more porous thrombolitic interior and the dense non-porous and micritic and layered stromatolitic structure is interpreted to represent a greater hiatus and slower growth during development of the outer rind. Dupraz *et al.* (2011) emphasized that a key factor in stromatolite genesis is repeated hiatuses and lithification of microbial biofilms, thus resulting in the development of a laminated structure. Furthermore, the outer contact of the rind in phase 1 and 3 of the intermediate to large scale mounds in the Point Peak are consistently onlapped by siliciclastic silt (indicating hiatuses) whereas stage 2 lacks a rind and intertongues with intermound sediment indicating more continuous growth.

Microbial mounds encapsulated by stromatolitic or micritic rinds have been widely reported from upper Cambrian microbialites (Shapiro and Awramik, 2000; Lee *et al.*, 2014; Coulson and Brand, 2016) and have been interpreted to be a global phenomenon (Rowland and Shapiro, 2002).

The biostromes within the lower Point Peak Member contain detrital carbonate and siliciclastic sediment trapped between clots whereas the large mounds of the upper Point Peak have little entrapped detrital material. This indicates that microbial micrite precipitation is the dominant mode of growth, with agglutination of detrital material playing a secondary role only in low-relief forms with a significant flux of detrital material onto the microbialite surface. The microbialites of the Point Peak are dominantly “fine grained” precipitated microbialites typical of the Palaeozoic in contrast to coarse agglutinate forms that are restricted to the Neogene and modern (Riding, 2011). The interior of intermediate and larger buildups is preferentially dolomitized when compared to the outer dense, micritic rind. The faster growth and greater depositional porosity in the mound interior may have led to greater permeability and preferential dolomitization.

Variations in external morphologies of microbial mounds in the Point Peak can be explained by competitive fitted growth of coalesced forms, or alignment of structures with current directions. Fitted structures of the biostromes in the lower Point Peak (Figure 12C) record column growth close to each other forming “compromise boundaries”. Intermediate to large mounds in the upper Point Peak are preferentially elongated in a NE-SW direction (Figure 9B; Khanna *et al.*, 2019) in alignment with tidal currents and directional oceanic currents (Figure 3; Khanna *et al.*, 2019). Elongation of microbial structures by differential accretion and erosion by tidal currents has been recognized and modelled from modern examples such as the subtidal stromatolites in Shark Bay (Bosak *et al.*, 2013; Suosaari *et al.*, 2016).

6.4 | Controls on oolite genesis

The ooids of the Morgan Creek and Point Peak members have normal sizes (<2 mm) similar to marine ooids from modern

depositional systems. The size of ooids has been interpreted to reflect seawater carbonate saturation state, with larger ooid sizes recording higher values, especially in the Proterozoic (Swett and Knoll, 1989; Sumner and Grotzinger, 1993) and Early Triassic (Lehrmann *et al.*, 2012). Extensive development of microbialites and flat-pebble conglomerates have been interpreted to indicate high seawater carbonate saturation during the Cambrian (Riding and Liang, 2005; Wright and Cherns, 2016). Thus, the lack of large ooids indicates that factors other than seawater carbonate-saturation state must have played a greater role in controlling ooid size during Point Peak deposition. Further work is needed to evaluate the numerous possibilities to explain the discrepancy such as biotic control on ooid size, differences in hydrodynamic conditions, the abundance of nuclei or the impact on ooid precipitation of vast epicratonic seas.

Oolite deposition in the Morgan Creek and Point Peak members presents similarities with modern oolite deposition in the Great Bahama Bank. Both systems record deposition in high-energy shoals at the seaward platform edge or outer shelf with vigorous agitation by tide and wave currents, redistribution of oolitic sands as finer-grained sheet-deposits with admixed mud and peloidal sediment (Harris *et al.*, 2019), and association of ooid shoals with large subtidal microbial structures (Dill *et al.*, 1986; Reid *et al.*, 1995; Feldmann and McKenzie, 1998; Reid *et al.*, 2003; Dupraz *et al.*, 2011). The two systems differ, however, in original mineralogical composition and microstructure. The oolites of the Morgan Creek and Point Peak members are characterized by radial cortical fabrics indicating an original Mg-calcite mineralogy and formation during the calcite sea conditions of the Late Cambrian (Wilkinson *et al.*, 1985; Chow and James, 1987b).

6.5 | Controls on depositional cyclicity

The low-frequency and intermediate-frequency cyclicity in the Morgan Creek and Point Peak members are interpreted to represent transgressive–regressive shifts in the shoreline driven by relative sea-level fluctuation. The approximately 3.5 Myr duration of the Sunwaptan Stage (ICS, 2019) places the cyclicity in the third and fourth temporal orders (Vail *et al.*, 1991). Fluctuation between nearshore and offshore facies associations is interpreted to represent lateral shifts of the shoreline and changes in siliciclastic input into the system and through the cycles (Figure 15).

The Morgan Creek and Point Peak members, however, lack any consistent high-frequency (5th order) shallowing-upward peritidal, or graining-upward subtidal cycles at the metre scale similar to those widely reported from Cambro-Ordovician peritidal successions (Demico, 1985; Koerschner and Read, 1989; Wilson *et al.*, 1991; Cowan and James, 1993; Goldhammer *et al.*, 1993; Fritz *et al.*, 2012).

In contrast, the metre-scale stratigraphic architecture of the Morgan Creek and Point Peak members consists of random shifts between the various facies (Figure 15 and Figure S1).

In the context of high-energy reworking of skeletal–oolitic–intraclastic sediment by storms, development of hiatuses in hardgrounds and erosion of channels, metre scale cyclicity is interpreted to be obscured by an incomplete record with numerous gaps and an episodic signal introduced by storms (Figure 15). The Morgan Creek and Point Peak record may be represented more by gap than by sediment accumulation (Ager, 1992). Other mechanisms that have been invoked to explain randomness in peritidal successions, such as “missed beats” in sea-level fluctuation or autocyclicity, do not offer likely explanations for the randomness, as the Cambrian was a green-house climate period with low-amplitude sea-level fluctuations unlikely to produce “missed beats”, and autocyclicity, despite introducing randomness, produces shallowing-upward cycles (Lehrmann and Goldhammer, 1999). The interpretation of an incomplete record for Cambrian deposition contrasts with Runkel *et al.* (2008) who interpreted a relatively complete record of epicratonic sedimentation despite low subsidence rates. Randomness, episodic deposition and gaps at the scale of high-frequency cycles in the Morgan Creek and Point Peak record of central Texas point to local oceanographic factors impacting the stratigraphic record.

7 | CONCLUSIONS

The facies of upper Morgan Creek and Point Peak members of the Wilberns Formation are interpreted to represent deposition on a broad, tide-dominated, mixed carbonate–siliciclastic ramp system influenced by storms. Aeolian delivery of siliciclastic sediment to the shoreline and spatial mixing of carbonate–siliciclastic sediments on the tidal flat is interpreted from textures and sedimentary structures of the sandstone–siltstone and heterolithic facies. Offshore oolitic and skeletal sand was deposited in shoals associated with large microbial mounds. Oolitic and skeletal sands as well as intraclastic conglomerate were reworked by storms.

Low-frequency and intermediate-frequency stratigraphic cycles were driven by transgressive–regressive shifts in the shoreline and changes in the rate of siliciclastic flux in response to relative sea-level fluctuation. The lack of cyclicity and randomness in facies succession at the metre scale are interpreted to reflect an incomplete record and episodic signal introduced by storms.

Microbialites formed both in the low-accommodation setting of the outer tidal flats and in the greater accommodation setting of offshore open-marine subtidal environments. Substrates for microbial growth are commonly subtidal hardgrounds and flat-pebble conglomerates. Biostromes are composed of coalesced thrombolitic mounds with dense

leolite or stromatolite rinds. Larger mounds are composed of stromatolitic columns enveloped in dense micritic and finely clotted thrombolitic rinds. Cauliflower to lobate, centimetre-scale, thrombolitic clots are composed of irregular microbial micrite or peloidal micrite. Millimetre-scale, finely clotted thrombolites are composed of calcimicrobial frameworks. The dense leolite to stromatolitic outer rind of thrombolites in biostromes, and the dense micritic finely clotted rind enclosing larger mounds are interpreted to represent slower growth and a greater hiatus on the outer surface of microbial structures. The internal component of mounds is commonly dolomitized, possibly as a result of greater original porosity.

Dominant controls on microbial genesis are interpreted to be accommodation space and modification by currents. Siliciclastic flux is interpreted to have played a relatively minor role in microbialite growth as biostromes and small mounds grew uninhibited by siliciclastic flux and trapped siliciclastic silt within their thrombolitic structures. The large offshore microbial mounds developed with minor entrapped siliciclastic sediment but contain a three-phase growth history in which pulses of siliciclastic flux impacted growth phases. External mound shape is influenced by competitive growth especially evident in coalesced mounds in biostromes. A dominant north-east orientation of intermediate and large-scale mounds in the upper Point Peak is interpreted to have been shaped by tidal currents.

Oolitic sediments show strong similarities to modern, outer platform oolite shoal deposits of the Great Bahama Bank, such as association with large subtidal microbial mounds, occurrence in tide agitated shoals and evidence of reworking of shoal sands into sheet deposits. Ooids have radial cortices indicating original Mg calcite mineralogy typical of a greenhouse calcite sea. Despite the fact that extensive microbialite development and other characteristics of the upper Cambrian lithofacies have previously been interpreted to indicate high seawater carbonate-saturation state, the ooids are similar in size to those of modern settings, with a notable lack of giant ooids, indicating that other factors must have competed with seawater carbonate-saturation state in controlling ooid size in this system.

ACKNOWLEDGEMENTS

We thank the Shepard and Zesch families for allowing us access to their ranches for conducting geologic fieldwork. We also thank ranch managers Mark and Priscilla Krause for their assistance and friendship while conducting the fieldwork. Robert Youens of Camerawings Inc. is acknowledged for the excellent job he did conducting an aerial photography survey of the field area. Financial support was provided by a joint industry project grant funded by Chevron, Conoco-Phillips, Shell, Statoil and Rice University Subcontract (grant/award number OTT-SRA-13-0182_Sub). The authors have no conflict of interests. We appreciate the very thorough and constructive reviews by

Peter Burgess, Brian Pratt and an anonymous reviewer that led to significant improvements of the manuscript.

DATA AVAILABILITY STATEMENT

The data that support the findings of this study are available from the corresponding author upon reasonable request.

ORCID

Daniel J. Lehrmann  <https://orcid.org/0000-0002-0838-3814>

Paul (Mitch) Harris  <https://orcid.org/0000-0002-6908-9088>

Pankaj Khanna  <https://orcid.org/0000-0001-7165-3082>

REFERENCES

- Ager, D.V. (1992) *The Nature of the Stratigraphical Record*, 3rd edition. Chichester: Wiley.
- Ahr, W.M. (1967) *Origin and palaeoenvironment of some Late Cambrian algal reefs, Mason County area, Texas*. PhD Thesis, Rice University.
- Ahr, W.M. (1971) Palaeoenvironment, algal structures, and fossil algae in the Late Cambrian of central Texas. *Journal of Sedimentary Petrology*, 41(1), 205–216.
- Allison, P.A. and Wells, M.R. (2006) Circulation in large ancient epicontinental seas: what was different and why? *Palaios*, 21, 513–515.
- Alvaro, J.J. and Clausen, S. (2007) Botoman (Lower Cambrian) turbid- and clear-water reefs and associated environments from the High Atlas, Morocco. In Alvaro, J.J., Aretz, M., Boulvain, F., Munnecke, A., Vachard, D. and Vennin, E. (Eds.), *Reefs and Bioaccumulations: Climate and Evolutionary Controls*. Geological Society of London, *Special Publication*, 275, 51–70.
- Barnes, V.E. and Bell, W.C. (1977) The Moore Hollow Group of central Texas. University of Texas, Austin, Bureau of Economic Geology, Report of Investigations, 88.
- Bohacs, K.M., Norton, I.O., Gilbert, D., Neal, J.E., Kennedy, M., Borkowski, W. *et al.* (2012) The accumulation of organic-matter-rich rocks within an earth systems framework: The integrated roles of plate tectonics, atmosphere, ocean, and biota through the Phanerozoic. In Roberts, D.G. and Bally, A.W. (Eds.) *Regional Geology and Tectonics: Principles of Geologic Analysis*. Amsterdam: Elsevier, pp. 647–678.
- Bosak, T., Knoll, A.H. and Petroff, A.P. (2013) The meaning of stromatolites. *Annual Review of Earth and Planetary Sciences*, 41, 21–44.
- Bradley, G.M., Redfern, J., Hodgetts, D., George, A.D. and Wach, G.D. (2018) The applicability of modern tidal analogues to pre-vegetation paralic depositional models. *Sedimentology*, 65, 2171–2201.
- Bridge, J., Barnes, V.E. and Cloud, P.E. Jr (1947) Stratigraphy of the Upper Cambrian, Llano Uplift, Texas. *Geological Society of America Bulletin*, 58, 109–123.
- Byers, C.W. and Dott, R.H. (1995) Sedimentology and depositional sequences of the Jordan Formation (Upper Cambrian), northern Mississippi Valley. *Journal of Sedimentary Research*, B65, 289–305.
- Chafetz, H.S. (2007) Paragenesis of the Morgan Creek Limestone, Late Cambrian central Texas: constraint on the formation of glauconite. *Deep Sea Research II*, 54, 1350–1363.
- Chafetz, H.S. and Reid, A. (2000) Syndepositional shallow-water precipitation of glauconitic minerals. *Sedimentary Geology*, 136, 29–42.
- Chow, N. and James, N.P. (1987a) Cambrian grand cycles: a northern Appalachian perspective. *Geological Society of American Bulletin*, 98, 418–429.

- Chow, N. and James, N.P. (1987b) Facies specific, calcitic and biminer-
al ooids from middle and upper Cambrian platform carbonates,
western Newfoundland, Canada. *Journal of Sedimentary Petrology*,
57(5), 907–921.
- Coulson, K.P. and Brand, L.P. (2016) Lithistid sponge-microbial
reef-building communities construct laminated, upper Cambrian
(Furongian) “Stromatolites”. *Palaios*, 31(7), 358–370.
- Cowan, C.A. and James, N.P. (1993) The interactions of sea-level
change, terrigenous-sediment influx, and carbonate produc-
tivity as controls on Late Cambrian grand cycles of western
Newfoundland, Canada. *Geological Society of America Bulletin*,
109, 16–42.
- Cowan, C.A. and James, N.P. (1996) Autogenic dynamics in carbon-
ate sedimentation of meter-scale shallowing-upward cycles, Upper
Cambrian, western Newfoundland, Canada. *American Journal of
Science*, 269, 1175–1207.
- Dalrymple, R.W. (2010) Tidal depositional systems. In: James, N.P. and
Dalrymple, R.W. (Eds.) *Facies Models: Geotext 6*. Newfoundland:
Geological Association of Canada, pp. 201–231.
- Demicco, R.V. (1985) Platform and off-platform carbonates of the
Upper Cambrian of western Maryland, U. S. A. *Sedimentology*, 32,
1–22.
- Demicco, R.V. and Hardie, L.A. (1995) Sedimentary structures and
early diagenetic features of shallow marine carbonate deposits.
SEPM Atlas, Series 1, Tulsa: SEPM.
- Dill, R.F., Shinn, E.A., Jones, A.T., Kelly, K. and Steinen, R.P. (1986)
Giant subtidal stromatolites forming in normal salinity waters.
Nature, 324, 55–58.
- Dott, R.H. Jr, Byers, C.W., Fielder, G.W., Stenzel, S.R. and Winfree,
K.E. (1986) Eolian to marine transition in Cambrian – Ordovician
cratonic sheet sandstones of the northern Mississippi Valley, U.S.A.
Sedimentology, 33, 345–367.
- Driese, S.G., Byers, C.W. and Dott, R.H. Jr (1981) Tidal deposition
in the basal Upper Cambrian Mt. Simon Formation in Wisconsin.
Journal of Sedimentary Petrology, 51, 367–381.
- Dupraz, C., Reid, P.R. and Visscher, P.T. (2011) *Microbialites, Modern*.
Encyclopedia of Earth Sciences Series. The Netherlands: Springer,
pp. 617–633. https://doi.org/10.1007/978-1-4020-9212-1_195
- Eoff, J.D. (2014) Sedimentary facies of the Upper Cambrian (Furongian;
Jingshanian and Sunwaptian) Tunnel City Group, Upper Mississippi
Valley: new insights on the old stormy debate. *Sedimentary Geology*,
302, 102–121.
- Feldmann, M. and McKenzie, J.A. (1998) Stromatolite–thrombolite as-
sociations in a modern environment, Lee Stocking Island, Bahamas.
Palaios, 13, 201–212.
- Flügel, E. (1982) *Microfacies Analysis of Limestones*. New York, NY:
Springer.
- Fritz, R.D., Medlock, P., Kuykendall, M.J. and Wilson, J.L. (2012) The
geology of the Arbuckle Group in the midcontinent: Sequence stratig-
raphy, reservoir development, and the potential for hydrocarbon explo-
ration. In Derby, J.R., Fritz, R.D., Longacre, S.A., Morgan, W.A. and
Sternbach, C.A. (Eds.), *The Great American Carbonate Bank: The
Geology and Economic Resources of the Cambrian — Ordovician
Sauk Megasequence of Laurentia*. *AAPG Memoir*, 98, 203–273.
- Ginsburg, R.N. (1982) Actualistic depositional models for the great
American bank (Cambro-Ordovician) (abs.). 11th International
congress on sedimentology. International Association of
Sedimentologists, p. 114.
- Ginsburg, R.N. and Planavsky, N.J. (2008) Diversity of Bahamian stro-
matolite substrates. In: Dilek, Y., Furnes, H. and Muehlenbachs, K.
(Eds.) *Links Between Geological Processes, Microbial Activities &
Evolution of Life*. Amsterdam, The Netherlands: Springer Academic
Press, pp. 177–195.
- Goldhammer, R.K., Lehmann, P.J. and Dunn, P.A. (1993) The origin of
high-frequency platform carbonate cycles and third-order sequences
(Lower Ordovician El Paso Gp., West Texas); constraints from
outcrop data and stratigraphic modelling. *Journal of Sedimentary
Research*, 63(3), 318–359.
- Harris, P.M. (2019) Lessons from a modern carbonate sandbody – a per-
sonal experience of comparative sedimentology. *The Depositional
Record*, 5, 1–13.
- Harris, P.M., Diaz, M.R. and Eberli, G.P. (2019) The formation and
distribution of modern ooids on Great Bahama Bank. *The Annual
Review in Marine Science*, 11, 491–516.
- ICS (2019) International commission on stratigraphy. Stratigraphy.org.
Accessed on 9-25-2019.
- Jones, K. and Surpless, K. (2018) Insights into the Precambrian Llano
Uplift from geochronology of the Cambrian Hickory Sandstone.
Geological Society of America Abstracts with Programs 50 (6).
<https://doi.org/10.1130/abs/2018AM-316035>
- Kelleher, C., Liu, J., Lhemann, A., Yazbek, L., Mercado, L., Lehrmann,
D., Hopson, H., Khanna, P. and Droxler, A.W. (2017) Environmental
and sequence stratigraphic control on microbialite morphology and
microfacies in a marine mixed carbonate siliciclastic system, Upper
Cambrian Point Peak Formation, Llano River and Mill Creek, Mason
County, central Texas. Geological Society of America Abstracts
with Programs, 49 (1). <https://doi.org/10.1130/abs/2017SC-288844>
- Khanna, P., Droxler, A.W., Hopson, H.H., Kubik, B., Proctor, J., Singh,
P. et al. (2019) Late Cambrian Microbial Buildups, Llano area, cen-
tral Texas: A 3 Phase Morphological Evolution. *Sedimentology*,
67(2), 1135–1160.
- Kiessling, W. (2009) Geologic and biologic controls on the evolution
of reefs. *Annual Review of Ecology, Evolution, and Systematics*, 40,
173–192.
- Klein, G.D. and Ryer, T.A. (1978) Tidal circulation patterns in
Precambrian, Paleozoic, and Cretaceous epeiric and mioclinal shelf
seas. *Geological Society of America Bulletin*, 89, 1050–1058.
- Koerschner, W.F. III and Read, J.F. (1989) Field and modelling studies
of Cambrian carbonate cycles, Virginia Appalachians. *Journal of
Sedimentary Petrology*, 59(5), 654–687.
- Krause, S.J. (1996) Stratigraphic framework, facies analysis, and dep-
ositional history of the Middle to Late Cambrian Riley Formation,
central Texas. Master’s thesis, University of Texas, Austin.
- Kyle, R.J. and McBride, E.F. (2012) Geology of the Voca frac sand dis-
trict, western Llano Uplift, Texas. Proceedings of the 48th Annual
Forum on the Geology of Industrial Minerals, Phoenix, Arizona.
Arizona Geological Survey Special Paper, 9 (2), 1–13.
- Labaj, M.A. and Pratt, B.R. (2016) Depositional dynamics in a mixed
carbonate-siliciclastic system: Middle-Upper Cambrian Abrigo
Formation, southeastern Arizona, U.S.A. *Journal of Sedimentary
Research*, 86, 11–37.
- Lee, J.H., Chen, J., Choh, S.J., Lee, D.J., Han, Z. and Chough, S.K.
(2014) Furongian (Late Cambrian) sponge-microbial maze-like
reefs in the North China Platform. *Palaios*, 29, 27–37.
- Lehrmann, D.J. and Goldhammer, R.K. (1999) Secular variation in fa-
cies and parasequence stacking patterns of platform carbonates: a
guide to application of the stacking patterns technique in strata of
diverse ages and settings. In Harris, P.M. and Simo, T.A. (Eds.),
Recent Advances in Carbonate Sequence Stratigraphy; Applications

- to Reservoirs, Outcrops and Models. *SEPM, Society for Sedimentary Geology, Special Publication*, 63, 187–226.
- Lehrmann, D.J., Minzoni, M., Payne, J., Li, X. and Yu, M. (2012) Lower Triassic oolites of the Nanpanjiang Basin: controls on facies architecture, giant ooids, marine cements and implications for hydrocarbon reservoirs. *American Association of Petroleum Geologists Bulletin*, 96(8), 1389–1414.
- Lochman-Balk, C. (1970) Late Cambrian faunal patterns on the craton. *Geological Society of America Bulletin*, 81, 3197–3224.
- MacNaughton, R.B., Hagadorn, J.W. and Dott, R.H. (2019) Cambrian wave-dominated tidal-flat deposits, central Wisconsin, USA. *Sedimentology*, 66, 1643–1672.
- Mancini, E.A., Morgan, W.A., Harris, P.M. and Parcel, W.C. (2013) Introduction: microbial carbonates, A Hedberg Conference issue. *American Association of Petroleum Geologists Bulletin*, 97(11), 1835–1847.
- McBride, E.F., Abdel-Wahab, A.A. and Milliken, K.L. (2002) Petrography and diagenesis of a half-billion-year-old cratonic sandstone (Hickory), Llano region. University of Texas, Austin, Bureau of Economic Geology, Report of Investigation.
- Miller, J.F., Loch, J.D. and Taylor, J.F. (2012) Biostratigraphy of Cambrian and Lower Ordovician strata in the Llano Uplift, central Texas. In Derby, J.R., Fritz, R.D., Longacre, S.A., Morgan, W.A. and Sternbach, C.A. (Eds.), *The Great American Carbonate Bank: The Geology and Economic Resources of the Cambrian–Ordovician Sauk Megasequence of Laurentia*. *AAPG Memoir* 98, 187–202.
- Morgan, W.A. (2012) Sequence stratigraphy of the Great American Carbonate Bank. In Derby, J.R., Fritz, R.D., Longacre, S.A., Morgan, W.A. and Sternbach, C.A. (Eds.), *The Great American Carbonate Bank: The Geology and Economic Resources of the Cambrian–Ordovician Sauk megasequence of Laurentia*. *AAPG Memoir*, 98, 37–79.
- Myrow, P.M., Tice, L., Archuleta, B., Clark, B., Taylor, J.F. and Ripperdan, R.L. (2004) Flat-pebble conglomerate: its multiple origins and relationship to metre-scale depositional cycles. *Sedimentology*, 51, 973–996.
- Palmer, A.R. (1981) Subdivision of the Sauk sequence. In Taylor, M.E. (Ed.), *Short Papers for the 2nd International Symposium on the Cambrian System*. U.S. Geological Survey Open File Report 81–743, 160–162.
- Palmer, A.R. (1989) Late Upper Cambrian shelf depositional facies and history, southern Missouri. In: Gregg, J.M., Palmer, J.R. and Kurtz, V.E. (Eds.) *Field Guide to the Upper Cambrian of Southeastern Missouri*. Geological Society of America, Annual Meeting Field Trip Guide, 1–24, pp. 1–24.
- Planavsky, N. and Ginsburg, R.N. (2009) Taphonomy of modern marine Bahamian microbialites. *Palaios*, 24, 5–17.
- Plint, A.G. (2010) Wave- and storm-dominated shoreline and shallow marine systems. In: James, N.P. and Dalrymple, R.W. (Eds.) *Facies Models: Geotext 6*. Newfoundland: Geological Association of Canada, pp. 167–199.
- Pratt, B.R. (2002) Storms versus tsunamis: Dynamic interplay of sedimentary, diagenetic, and tectonic processes in the Cambrian of Montana. *Geology*, 30(5), 423–426.
- Pratt, B.R. (2010) Peritidal carbonates. In: James, N.P. and Dalrymple, R.W. (Eds.) *Facies Models: Geotext 6*. Newfoundland: Geological Association of Canada, pp. 401–420.
- Pratt, B.R. and Bordonaro, O.L. (2007) Tsunamis in a stormy sea: Middle Cambrian inner-shelf limestones of western Argentina. *Journal of Sedimentary Research*, 77, 256–262.
- Pratt, B.R. and Ponce, J.J. (2019) Sedimentation, earthquakes, and tsunamis in a shallow, muddy epeiric sea: Grinnell Formation (Belt Supergroup, ca. 1.45 Ga), western North America. *Geological Society of America Bulletin*, 131(9–10), 1411–1439.
- Proctor, J.M., Droxler, A.W., Derzhi, N., Hopson, H.H., Harris, P.M., Khanna, P. et al. (2019) Upscaling lithology and porosity type fractions from the micro- to the core-scale with thin-section petrography, dual energy computed tomography, and rock typing: creation of diagenesis and porosity-type logs. *AAPG/SEG Interpretation*, 7(1), B9–B32.
- Reid, R.P., Macintyre, I.G., Browne, K.M., Steneck, R.S. and Miller, T. (1995) Modern marine stromatolites in the Exuma Cays, Bahamas: uncommonly common. *Facies*, 33, 1–18.
- Reid, R.P., James, N.P., Macintyre, I.G., Dupraz, C.P. and Burne, R.V. (2003) Shark Bay stromatolites: microfibrils and reinterpretation of origins. *Facies*, 49, 299–324.
- Reijmer, J.J.G. (2014) *Carbonate Factories: Encyclopedia of Marine Geosciences*. The Netherlands, Springer Science, 1–8. https://doi.org/10.1007/978-94-007-6644-0_136-1
- Riding, R. (2006) Microbial carbonate abundance compared with fluctuations in metazoan diversity over geological time. *Sedimentary Geology*, 185, 229–238.
- Riding, R. (2011) Microbialites, stromatolites, and thrombolites. In: Reitner, J. and Thiel, V. (Eds.) *Encyclopedia of Geobiology*. Encyclopedia of Earth Science Series. Heidelberg: Springer, pp. 635–654.
- Riding, R. and Liang, L. (2005) Seawater chemistry control of marine limestone accumulation over the last 550 million years. *Revista Española de Micropaleontología*, 37(1), 1–11.
- Riegl, B., Poiriez, A., Janson, X. and Bergman, K.L. (2010) The gulf: facies belts, physical, chemical, and biological parameters of sedimentation on a carbonate ramp. In: Westphal, H., Riegl, B. and Eberli, G. (Eds.) *Carbonate Depositional Systems: Assessing Dimensions and Controlling Parameters*. Dordrecht: Springer, pp. 145–213.
- Rowland, S.M. and Shapiro, R.S. (2002) Reef patterns and environmental influences in the Cambrian and earliest Ordovician. In: Kiessling, W. and Flügel, E. (Eds.), *Phanerozoic Reef Trends*. *SEPM Special Publication*, 72, 95–128.
- Runkel, A.C., Miller, J.F., McKay, R.M., Palmer, A.R. and Taylor, J.F. (2007) High-resolution sequence stratigraphy of lower Paleozoic sheet sandstones in central North America: The role of special conditions of cratonic interiors in development of stratal architecture. *Geological Society of America Bulletin*, 119(7/8), 860–881.
- Runkel, A.C., Miller, J.F., McKay, R.M., Palmer, A.R. and Taylor, J.F. (2008) The record of time in cratonic interior strata: Does exceptionally slow subsidence necessarily result in exceptionally poor stratigraphic completeness? In Pratt, B.R. and Holmden, C. (Eds.), *Dynamics of Epeiric Seas: Sedimentological, Paleontological and Geochemical Perspectives*. *Geological Association of Canada Special Paper*, 48, 341–362.
- Runkel, A.C., McKay, R.M., Cowan, C., Miller, J.F. and Taylor, J.F. (2012) The sauk megasequence in the cratonic interior of North America: Interplay between a fully developed inner detrital belt and the central Great American Carbonate Bank. In Derby, J.R., Fritz, R.D., Longacre, S.A., Morgan, W.A. and Sternbach, C.A. (Eds.), *The Great American Carbonate Bank: The Geology and Economic Resources of the Cambrian–Ordovician Sauk Megasequence of Laurentia*. *AAPG Memoir*, 98, 37–79.
- Ruppel, S.C. and Kerans, C. (1987) Paleozoic buildups and associated facies, Llano Uplift, central Texas. Austin Geological Society, Guidebook 10.

- Schlager, W. (2000) Sedimentation rates and growth potential of tropical, cool-water and mud-mound carbonate systems. In: Insalaco, E., Skelton, P.W. and Palmer, T.J. (Eds.) *Carbonate Platform Systems: Components and Interactions*. London: The Geological Society, pp. 217–227.
- Schlager, W. (2003) Benthic carbonate factories of the Phanerozoic. *International Journal of Earth Sciences*, 92, 445–464.
- Shapiro, R.S. and Awramik, S.M. (2000) Microbialite morphostratigraphy as a tool for correlating Late Cambrian–Early Ordovician sequences. *Journal of Geology*, 108, 171–180.
- Shapiro, R.S. and Awramik, S.M. (2006) Favosamaceria cooperi, new group and form: A widely dispersed, time-restricted thrombolite. *Journal of Paleontology*, 80, 411–422.
- Shinn, E.A. (1983) Tidal flat environment. In Scholle, P.A., Bebout, G. and Moore, C.H. (Eds.) *Carbonate Depositional Environments*. Tulsa, American Association of Petroleum Geologists Memoir, 33, 173–210.
- Shinn, E.A. (1986) Modern carbonate tidal flats: their diagnostic features. *Quarterly Journal of the Colorado School of Mines*, 81, 7–35.
- Sliger, K.L. (1955) Geology of the Lower James river area. Master's Thesis, Texas A. & M. College.
- Spencer, R.J. and Demicco, R.V. (2002) Facies and stratigraphy of two Cambrian grand cycles: implications for Cambrian sea level and origin of grand cycles. *Bulletin of Canadian Petroleum Geology*, 50(4), 478–491.
- Spincer, B.R. (1997) The palaeoecology of some Late Cambrian reefs from central Texas, The great basin and Colorado, USA. PhD Thesis, University of Cambridge.
- Sumner, D. and Grotzinger, J.P. (1993) Numerical modelling of ooid size and the problem of Neoproterozoic giant ooids. *Journal of Sedimentary Petrology*, 63(5), 974–982.
- Suosaari, E.P., Reid, R.P., Playford, P.E., Foster, J.S., Stolz, J.F., Casaburi, G. et al. (2016). New multi-scale perspectives on the stromatolites of Shark Bay, Western Australia. *Scientific Reports*, 6, 20557. <https://doi.org/10.1038/srep20557>
- Swartz, H., Lehrmann, D., Kelleher, C., Lhemann, A., Suarez, M., Hopson, H. et al. (2017) Stable isotope and elemental geochemistry reveal environmental controls and diagenetic modification of microbialite facies within a sequence stratigraphic framework, Upper Cambrian Point Peak Formation, Llano River and Mill Creek, Mason County, central Texas. AAPG National meeting, Houston TX. AAPG Datapages/Search and Discovery Article, 90291.
- Swett, K. and Knoll, A.H. (1989) Marine pisolites from upper Proterozoic carbonates of East Greenland and Spitsbergen. *Sedimentology*, 36(1), 75–93.
- Tape, C.H., Cowan, C.A. and Runkel, A.C. (2003) Tidal-bundle sequences in the Jordan sandstone (Upper Cambrian), southeastern Minnesota, U.S. A.: Evidence for tides along inboard shorelines of the Sauk epicontinental sea. *Journal of Sedimentary Research*, 73(3), 354–366.
- Trower, E.J., Lamb, M.P. and Fischer, W.W. (2017) Experimental evidence that ooid size reflects a dynamic equilibrium between rapid precipitation and abrasion rates. *Earth and Planetary Science Letters*, 468, 112–118.
- Vail, P.R., Audemard, F., Bownam, S.A., Eisner, P.N. and Perez-Cruz, C. (1991) The stratigraphic signatures of tectonics, eustasy and sedimentology: an overview. In: Einsele, G. (Ed.) *Cycles and Events in Stratigraphy*. Berlin: Springer, pp. 617–659.
- Van Sicken, D.C. (1958) Depositional topography—examples and theory. *American Association of Petroleum Geologists Bulletin*, 42, 1897–1913.
- Westrop, S.R. (1989) Facies anatomy of an Upper Cambrian grand cycle: Bison Creek and Mistaya formations, southern Alberta. *Canadian Journal of Earth Sciences*, 26, 2292–2304.
- Wilkinson, B.H., Owen, R.M. and Carroll, A.R. (1985) Submarine weathering, global eustasy, and carbonate polymorphism in Phanerozoic marine oolites. *Journal of Sedimentary Petrology*, 55, 171–183.
- Wilson, J.L. (1967) Cyclic and reciprocal sedimentation in Virgilian strata of Southern New Mexico. *Geological Society of America Bulletin*, 78, 805–818.
- Wilson, J.L. (1994) The Lower Ordovician of the Great American Bank of the southwestern United States. In Keller, D.R. and Reed, C. (Eds.), *Paleokarst, Karst-Related Diagenesis, Reservoir Development, and Exploration Concepts: Examples from the Paleozoic Section of the southern Mid-Continent*. SEPM Guidebook. 93–34, 35–43.
- Wilson, J.L., Fritz, R.D. and Medlock, P.L. (1991) The Arbuckle Group—relationship of core and outcrop analysis to cyclic stratigraphy and correlation. In: Johnson, K.S. (Ed.) *Arbuckle Group Core Workshop and Field trip*. Oklahoma Geological Survey Special Publication 91–3, pp. 133–144.
- Wright, V.P. and Cherns, L. (2016) How far did feedback between biodiversity and early diagenesis affect the nature of Early Palaeozoic sea floors? *Palaeontology*, 59, 753–765.
- Zeccin, M. and Catuneanu, O. (2017) High-resolution sequence stratigraphy of clastic shelves VI: Mixed siliciclastic-carbonate systems. *Marine and Petroleum Geology*, 88, 712–723.

SUPPORTING INFORMATION

Additional supporting information may be found online in the Supporting Information section.

How to cite this article: Lehrmann DJ, Droxler AW, Harris P, et al. Controls on microbial and oolitic carbonate sedimentation and stratigraphic cyclicity within a mixed carbonate-siliciclastic system: Upper Cambrian Wilberns Formation, Llano Uplift, Mason County, Texas, USA. *Depositional Rec.* 2020;6:276–308. <https://doi.org/10.1002/dep2.108>